Eur. Phys. J. C 53, 367–384 (2008)
DOI 10.1140/epjc/s10052-007-0466-5

THE EUROPEAN PHYSICAL JOURNAL C

Regular Article – Theoretical Physics

The role of the quark and gluon GPDs in hard vector-meson electroproduction

S.V. Goloskokov[1], P. Kroll[2,a]

[1] Bogoliubov Laboratory of Theoretical Physics, Joint Institute for Nuclear Research, Dubna 141980, Russia
[2] Fachbereich Physik, Universität Wuppertal, Gaußstrasse 20, 42097 Wuppertal, Germany

Received: 19 September 2007 /
Published online: 27 November 2007 –

Abstract. Electroproduction of light vector mesons is analyzed on the basis of handbag factorization. The required generalized parton distributions are constructed from the CTEQ6 parton distributions with the help of double distributions. The partonic subprocesses are calculated within the modified perturbative approach. The present work extends our previous analysis of the longitudinal cross section to the transverse one and other observables related to both the corresponding amplitudes. Our results are compared to recent experimental findings in detail.

1 Introduction

In a previous work [1] we analyzed electroproduction of light vector mesons ($V = \rho^0, \phi, \omega$) at HERA kinematics within the handbag factorization scheme, which is based on generalized parton distributions (GPDs) and hard partonic subprocesses. The latter are calculated within the modified perturbative approach [2] in which the quark transverse momenta are retained. The emission and reabsorption of partons from the proton is still treated in collinear approximation. In the kinematical region accessible to the HERA experiments that is characterized by a Bjorken-x ($x_{\rm Bj}$) of the order 10^{-3}, it is not unjustified to restrict oneself to the gluonic subprocess $\gamma^* g \to V g$ and the associated gluonic GPD H^g. In a recent paper [3] we extended that analysis to larger values of $x_{\rm Bj}$ ($\lesssim 0.2$) such as accessible to the HERMES experiment, but restricting ourselves to the analysis of the least model-dependent amplitude, namely the one for transitions from longitudinal polarized virtual photons to vector mesons polarized in the same manner, $\gamma^*_{\rm L} p \to V_{\rm L} p$. This analysis necessitates the inclusion of the quark subprocesses $\gamma^* q \to V q$ (see Fig. 1) and the associated GPDs for sea and valence quarks.

In this work we are going to complete the analysis of vector-meson electroproduction by studying the amplitude for transversely polarized photons and mesons, $\gamma^*_{\rm T} p \to V_{\rm T} p$. The basic idea of modeling this amplitude has been already described in [1] for the gluonic contribution. The extension to the quark contribution is straightforward. The crucial point at issue with the transverse amplitude is that the quark transverse momenta, which are retained in the modified perturbative approach in order to suppress configurations with large transverse separations of the quark and antiquark forming the meson, regularize the infrared singularities occurring in the transverse subprocess amplitude in collinear approximation [4,5] at the same time. These special configurations seem to be responsible for the excess of the leading-twist contribution to the longitudinal cross section over experiment. Indeed, taking into account the quark transverse momenta, fair agreement between theory and experiment is achieved [3]. We are going to apply this modified handbag approach to vector-meson electroproduction for energies, W, in the photon–proton center of mass system (c.m.s.) between about 5 and 170 GeV and photon virtualities, Q^2, between about 3 and 100 GeV^2, while $x_{\rm Bj}$ is less than $\lesssim 0.2$. We will compare our results in detail with recent data from HERA, COMPASS and HERMES.

The GPDs H for quarks and gluons, which dominate the process of interest for unpolarized protons at small $x_{\rm Bj}$, are constructed from the CTEQ6 parton distribution functions (PDFs) [6] through double distributions [7,8]. Applying the same model to the GPDs $\widetilde{H}$, we are also going to estimate the so-called unnatural parity amplitudes and to study their implications on spin density matrix elements (SDMEs) and the double spin asymmetry $A_{\rm LL}$ describing the correlation of the helicities of the beam and target particles.

In [9] the electromagnetic form factors of the nucleon have been used to extract the zero-skewness GPDs H, $\widetilde{H}$ and E for valence quarks. The forward limit of $E^{\rm a}_{\rm val}$, the analog of the PDFs, determined in [9], can be utilized for the construction of $E^{\rm a}_{\rm val}$ at non-zero skewness with the double distribution model. With these GPDs at our disposal we will also estimate the SDMEs measurable with a transversely polarized target as well as the transverse spin asymmetry A_{UT}.

The plan of the paper is as follows: in Sect. 2 we will sketch the modified handbag approach. In Sect. 3 the dou-

[a] e-mail: kroll@physik.uni-wuppertal.de

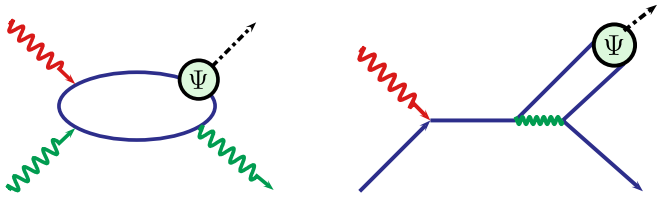

Fig. 1. Typical lowest order Feynman graphs for the $\gamma^* g \to V g$ (*left*) and $\gamma^* q \to V q$ (*right*) subprocesses of meson electroproduction

ble distribution model for the GPD H is described. The results on cross sections and SDMEs obtained within the handbag approach are presented in Sects. 4 and 5, respectively. Section 6 is devoted to an estimate of the role of the GPDs $\widetilde{H}$ and Sect. 7 to that of the GPDs E. We will conclude this paper by a summary (Sect. 8).

2 The handbag approach

We are interested in vector-meson electroproduction in a kinematical region characterized by large Q^2 and large W but small $x_{\rm Bj}$ ($\lesssim 0.2$) and small invariant momentum transfer $-t$. In the handbag approach, the amplitudes for the process $\gamma^* p \to V p$, which can be extracted from vector-meson electroproduction applying the one-photon approximation, factorize into partonic subprocesses (see Fig. 1) and GPDs comprising the soft, non-perturbative QCD. At large Q^2 the amplitude for $\gamma^*_{\rm L} p \to V_{\rm L} p$ dominates and factorization has been shown to hold for it rigorously [10, 11]. The amplitudes for other photon–meson transitions are suppressed by inverse powers of Q. Besides the longitudinal amplitude we will consider only the transverse one, $\gamma^*_{\rm T} p \to V_{\rm T} p$ in this work, which is the most important one of the suppressed amplitudes at small $-t$. Proton helicity flip is suppressed by $\sqrt{-t}/2m$ (m being the proton's mass) and can be neglected in calculations of cross sections and SDMEs obtained with unpolarized protons. In Sect. 7 we will however estimate the size of the proton helicity-flip amplitudes explicitly. It will turn out that these amplitudes are indeed small.

In the region of small $x_{\rm Bj}$ the dominant contributions are provided by the GPD H. To the proton helicity-non-flip amplitude the GPDs contribute in the combination

$$H - \frac{\xi^2}{1-\xi} E \,, \tag{1}$$

where the skewness ξ is related to $x_{\rm Bj}$ by

$$\xi \simeq \frac{x_{\rm Bj}}{2 - x_{\rm Bj}} \left[1 + m_V^2/Q^2\right] . \tag{2}$$

Here, m_V denotes the mass of the vector meson. The GPD E can therefore safely be ignored, since it is not expected that it is much larger than the GPD H; see Sect. 7, where we will take up this issue again. The GPD $\widetilde{H}$ only contributes to the transverse amplitude and can also be neglected in calculations of the cross sections. In Sect. 6 we will return to this problem and estimate the size of its contribution. Since there is no parton helicity flip in the partonic subprocesses to the accuracy we are calculating them, the parton helicity-flip GPDs [12] do not occur.

The contributions from H to the $\gamma^* p \to V p$ amplitudes read ($i = g, q$, $x_g = 0$ and $x_q = -1$)

$$\mathcal{M}^{Ni}_{\mu+,\mu+}(V) = \frac{e}{2} \sum_a e_a \mathcal{C}^{\rm a}_V \times \int_{\bar{x}_i}^1 {\rm d}\bar{x} \sum_\lambda \mathcal{H}^{Vi}_{\mu\lambda,\mu\lambda}(\bar{x},\xi,Q^2,t=0) H^i(\bar{x},\xi,t) \,. \tag{3}$$

The first sum runs over the quark flavors a and e_a denotes the quark charges in units of the positron charge e. The non-zero flavor weight factors, $\mathcal{C}^a_V$, read

$$\mathcal{C}^u_\rho = -\mathcal{C}^d_\rho = \mathcal{C}^u_\omega = \mathcal{C}^d_\omega = 1/\sqrt{2} \,, \qquad \mathcal{C}^s_\phi = 1 \,. \tag{4}$$

The explicit helicities in (3) refer to the proton, while μ is the helicity of the photon and meson and λ that of the partons participating in the subprocess. Only the t dependence of the GPDs is taken into account in the amplitudes (3). That of the subprocess amplitudes $\mathcal{H}$ provides corrections of order t/Q^2, which we neglect throughout this paper. In contrast to the subprocess amplitudes the t dependence of the GPDs is scaled by a soft parameter, actually by the slope of the diffraction peak.

There is a minimal value of $-t$ allowed in the process of interest

$$t_{\rm min} = -4m^2 \frac{\xi^2}{1-\xi^2} \,. \tag{5}$$

As are other effects of order ξ^2 (e.g. the GPD E), the $t_{\rm min}$ effect is neglected. We note in passing that our helicities are light-cone ones, which naturally occur in the handbag approach. The differences to the usual c.m.s. helicities are of order $m\sqrt{-t}/W^2$ [12] and can be ignored in the kinematical region of interest in this work.

The full amplitude is given by a superposition of the gluon and quark contributions:

$$\mathcal{M}^N = \mathcal{M}^{Ng} + \mathcal{M}^{Nq} \,, \tag{6}$$

and it is normalized such that the partial cross sections for $\gamma^* p \to V p$ read (Λ is the usual Mandelstam function)

$$\frac{{\rm d}\sigma_{\rm L(T)}}{{\rm d}t} = \frac{1}{16\pi (W^2 - m^2)\sqrt{\Lambda(W^2, -Q^2, m^2)}} \times |\mathcal{M}^N_{0(+)+,0(+)+}|^2 \,, \tag{7}$$

which holds with regard to the above-mentioned simplifications. The cross sections integrated over t are denoted by $\sigma_{\rm L}$ and $\sigma_{\rm T}$. The full (non-separated) cross section for $\gamma^* p \to V p$ is

$$\sigma = \sigma_{\rm T} + \varepsilon \sigma_{\rm L} \,, \tag{8}$$

in which ε is the ratio of longitudinal to transverse photon fluxes. The power corrections of kinematical origin given

in (2) and in the phase space factor (7) are taken into account. With the exception of these kinematical effects hadron masses are omitted otherwise. In the expression (7) for the cross section the symmetry relation

$$\mathcal{M}^{Ni}_{-\mu\nu',-\mu\nu} = \mathcal{M}^{Ni}_{\mu\nu',\mu\nu} \tag{9}$$

has been used, which is an obvious consequence of the definition (3) and of parity conservation. This symmetry relation coincides with the one that holds for natural parity exchanges; we therefore mark this amplitude by a superscript N. Since the contributions from H to the amplitudes obey the relation

$$\mathcal{M}^{Ui}_{-\mu\nu',-\mu\nu} = -\mathcal{M}^{Ui}_{\mu\nu',\mu\nu}\,, \tag{10}$$

there are no interference terms between $\mathcal{M}^{Ni}$ and $\mathcal{M}^{Ui}$ in the observables for unpolarized electroproduction of vector mesons as can easily be shown. Equation (10) is also obtained for the exchange of a particle with unnatural parity. In analogy to the contributions from H the amplitudes related to $\widetilde{H}$ are marked by the superscript U. The contribution $|\,\mathcal{M}^U\,|^2$ is neglected in (7).

Let us now turn to the discussion of the subprocess amplitudes. As is well known, for the kinematics accessible to current experiments, the handbag amplitude evaluated in collinear approximation overestimates the longitudinal cross section although with the tendency of approaching experiment with increasing Q^2 [1, 13, 14]. One may wonder whether higher order perturbative QCD corrections to the subprocesses may cure that deficiency. However, this does not seem to be the case. NLO corrections [15, 16] are very large due to BFKL-type logarithms $\sim \ln 1/\xi$ and cancel to a large extent the LO term at low Q^2 and low $x_{\rm Bj}$. A recent attempt [17] to resum higher orders with methods known from deep inelastic lepton–nucleon scattering [18] seems to indicate that the sum of all higher order corrections to the LO term is not large. In view of this unsettled situation it seems to be reasonable to proceed along the lines advocated in [1, 3] by simply using the LO result and add power corrections, especially since such corrections are anyway needed in order to account for the large transverse cross section $\sigma_{\rm T}$. Once the higher order perturbative corrections are better understood within the modified perturbative approach one may add them to the LO results. As long as they are of reasonable magnitude there is no principal difficulty in this. It may merely be necessary to readjust the GPDs and the meson wave functions appropriately.

As in our papers [1, 3] we will model the required power corrections by employing the modified perturbative approach [2] in the calculation of the subprocesses. In this approach the transverse momenta of the quark and antiquark, $\mathbf{k}_\perp$ (defined with respect to the meson's momentum), entering the meson are kept. In contrast to the situation at the mesonic vertex, the partons entering the subprocess, are viewed as being emitted and reabsorbed by the proton collinearly. This scenario is supported by the fact that the GPDs describe the full proton, and their $\mathbf{k}_\perp$ dependence therefore reflects the proton's charge radius ($\langle \mathbf{k}_\perp^2 \rangle^{1/2} \simeq 200\,\text{MeV}$), while the meson is generated through its compact valence Fock state with a r.m.s. $\mathbf{k}_\perp$ of about 500 MeV [19, 20]. Instead of a meson's distribution amplitude allowance is to be made for a meson light-cone wave function $\Psi_{V\rm L}(\tau, k_\perp)$ in the modified perturbative approach [19, 20]. Here τ is the fraction of the light-cone plus component of the meson's momentum, q', the quark carries; the antiquark carries the fraction $\bar\tau = 1-\tau$. Quark transverse momenta are accompanied by gluon radiation. In [2] the gluon radiation has been calculated in the form of a Sudakov factor $\exp[-S(\tau, \mathbf{b}, Q^2)]$ to next-to-leading-log approximation using resummation techniques and having recourse to the renormalization group. The quark–antiquark separation, $\mathbf{b}$, in configuration space acts as an infrared cut-off parameter. Radiative gluons with wave lengths between the infrared cut-off and a lower limit (related to the hard scale Q^2) yield suppression; softer gluons are part of the meson wave function, while harder ones are an explicit part of the subprocess amplitude. Congruously, the factorization scale is given by the quark–antiquark separation, $\mu_{\rm F} = 1/b$, in the modified perturbative approach [2, 3].

Since the resummation of the logarithms involved in the Sudakov factor can only efficiently be performed in the impact parameter space [2] we have to Fourier transform the lowest order subprocess amplitudes to that space and to multiply them with the Sudakov factor there. This leads to

$$\mathcal{H}^{Vi}_{\mu\lambda,\mu\lambda} = \int \mathrm{d}\tau\, \mathrm{d}^2 b\, \hat\Psi_{V\rm L}(\tau, -\mathbf{b}) \hat{\mathcal{F}}^i_{\mu\lambda,\mu\lambda}(\bar x, \xi, \tau, Q^2, \mathbf{b}) \times \alpha_{\rm s}(\mu_R) \exp\left[-S\left(\tau, \mathbf{b}, Q^2\right)\right]. \tag{11}$$

The two-dimensional Fourier transformation between the canonically conjugated $\mathbf{b}$ and $\mathbf{k}_\perp$ spaces is defined by

$$\hat f(\mathbf{b}) = \frac{1}{(2\pi)^2} \int \mathrm{d}^2\mathbf{k}_\perp \exp\left[-\mathrm{i}\mathbf{k}_\perp\cdot\mathbf{b}\right] f(\mathbf{k}_\perp)\,. \tag{12}$$

The renormalization scale $\mu_{\rm R}$ is taken to be the largest mass scale appearing in the hard scattering amplitude, i.e. $\mu_{\rm R} = \max(\tau Q, \bar\tau Q, 1/b)$. Since the bulk of the handbag contribution to the amplitudes is accumulated in regions where $\mu_{\rm R}$ is smaller than 3 GeV we have to deal with three active flavors. A value of 220 MeV for $\Lambda_{\rm QCD}$ is used in the Sudakov factor and in the evaluation of $\alpha_{\rm s}$ from the one-loop expression.

The hard scattering kernels $\mathcal{F}^i$ or their Fourier transform $\hat{\mathcal{F}}^i$ occurring in (11) are computed from the pertinent Feynman graphs; see Fig. 1. The result for the gluonic subprocess is discussed in some detail in [1], and we refrain from repeating the lengthy expressions here. For quarks, on the other hand, the hard scattering kernel for longitudinally polarized photons and mesons reads

$$\mathcal{F}^q_{0+,0+} + \mathcal{F}^q_{0-,0-} = -C_{\rm F}\sqrt{\frac{2}{N_c}}\frac{Q}{\xi}\left[T_s - T_u\right], \tag{13}$$

where N_c denotes the number of colors and $C_{\rm F} = (N_c^2 - 1)/(2N_c)$ is the usual color factor. For convenience we only quote the sum over the quark helicities, since this is what appears in (3). The denominators of the parton propaga-

tors read

$$T_s = \frac{1}{k_\perp^2 - \tau(\bar{x}-\xi)Q^2/(2\xi) - \mathrm{i}\epsilon}\,,$$
$$T_u = \frac{1}{k_\perp^2 + \bar{\tau}(\bar{x}+\xi)Q^2/(2\xi) - \mathrm{i}\epsilon}\,. \qquad (14)$$

In both the quark and the gluon propagators we only retain $k_\perp$ in the denominators of the parton propagators, where it plays a crucial role. Its square competes with terms $\propto \tau(\bar{\tau})Q^2$, which become small in the end-point regions where either τ or $\bar{\tau}$ tends to zero.

While for longitudinally polarized vector mesons the transverse momentum of the quark is only needed for the suppression of the leading-twist contribution (the $\mathbf{k}_\perp \to 0$ limit), it plays an even more important role in the case of transverse polarization. In the collinear limit the spin wave function of the meson is $\Gamma_V \propto \not{q}' \not{\epsilon}_V(\pm 1)$, where ϵ_V denotes the polarization vector of the meson. It, however, leads to a vanishing contribution to the subprocess amplitude, since the number of γ matrices in the Dirac trace[1] that gives the hard scattering kernel is odd (see Fig. 1).[2] If one allows for quark transverse momenta a second term in the covariant spin wave function appears

$$\Delta\Gamma_V^\nu K_\nu = \frac{1}{\sqrt{2}M_V}\{\not{q}'\not{\epsilon}_V, \gamma_\nu\}K^\nu\,, \qquad (15)$$

for which the number of γ matrices in the Dirac trace is even. In (15) M_V is a soft parameter of the order of the vector-meson mass, e.g. a typical constituent quark mass. The transverse momentum four-vector $K = [0, 0, \mathbf{k}_\perp]$ is suitably defined as the quark–antiquark relative momentum and represents one unit of orbital angular momentum in a covariant manner [1]. Expanding now the hard scattering kernel for transversely polarized vector mesons, one finds

$$\begin{aligned}\mathcal{F}^i_{+\lambda,+\lambda}(\xi,\bar{x},\tau,Q^2,K) = {}& \mathcal{F}^i_{+\lambda,+\lambda}(\xi,\bar{x},\tau,Q^2,\mathbf{k}_\perp^2)\\ &+ \Delta\mathcal{F}^{i\,\nu}_{+\lambda,+\lambda}(\xi,\bar{x},\tau,Q^2,\mathbf{k}_\perp^2)K_\nu\\ &+ \Delta\mathcal{F}^{i\,\nu\mu}_{+\lambda,+\lambda}(\xi,\bar{x},\tau,Q^2,\mathbf{k}_\perp^2)K_\nu K_\mu\\ &+ \ldots \qquad (16)\end{aligned}$$

Higher order terms in K_μ are neglected. In the spirit of the modified perturbative approach, the $\mathbf{k}_\perp^2$ terms in the propagator denominators are kept, as has been done for the longitudinal amplitude. As already mentioned the first term in (16), generated by $\not{q}'\not{\epsilon}_V(\pm 1)$ vanishes as a consequence of the number of γ matrices in the trace and, evidently, the second one as well after integration on $\mathbf{k}_\perp$. Hence, the third term in (16) is the leading one for transversely polarized mesons and leads to the subprocess amplitudes

$$\mathcal{H}^{Vi}_{+\lambda,+\lambda} = -\frac{g_{\perp\mu\nu}}{2}\int \mathrm{d}\tau\,\frac{\mathrm{d}\mathbf{k}_\perp^2}{16\pi^2}\mathbf{k}_\perp^2\Psi_{V\mathrm{T}}(\tau,\mathbf{k}_\perp^2)\,\Delta\mathcal{F}^{i\nu\mu}_{+\lambda,+\lambda}\,, \qquad (17)$$

in which $g_\perp$ is the transverse metric tensor.[3] Note that the wave functions for longitudinally and transversely polarized vector mesons are different in general. The transverse amplitude is of order $\mathbf{k}_\perp^2/(M_V Q)$. Noting that $\langle\mathbf{k}_\perp^2\rangle^{1/2}/M_V$ is of order unity, one realizes that the transverse amplitude is suppressed by

$$\mathcal{M}_{+\nu',+\nu} \propto \langle\mathbf{k}_\perp^2\rangle^{1/2}/Q\,, \qquad (18)$$

with respect to the one for longitudinally polarized vector mesons.

Working out the kernels, one finds after summation over the parton helicity that the kernel for transverse photon and meson polarization is obtained from the longitudinal one, (13), by the replacement

$$T_s - T_u \longrightarrow \frac{\mathbf{k}_\perp^2}{2}\,\frac{Q}{M_V}\,[T_s T_a - T_u T_b]\,. \qquad (19)$$

The new propagator denominators read

$$T_a = \frac{1}{\tau Q^2 + \mathbf{k}_\perp^2}\,, \qquad T_b = \frac{1}{\bar{\tau}Q^2 + \mathbf{k}_\perp^2}\,. \qquad (20)$$

We note in passing that T_s and T_u represent the denominators of the gluon propagators in the LO subprocess $\gamma^* q \to V q$, while T_a and T_b belong to the quark propagators (see Fig. 1). With the help of partial fractioning ($i = s, u$ and $j = a, b$)

$$T_i T_j = \frac{1}{\mathbf{k}_\perp^2}\,[c_i T_i + c_j T_j]\,, \qquad (21)$$

we can cast the Fourier transform of the transverse subprocess amplitude into exactly the same form as for the longitudinal one, (11). The kernel is then a linear combination of four Fourier transformed propagators.

The denominators of the parton propagators in (14) are either of the type

$$T_1 = \frac{1}{\mathbf{k}_\perp^2 + d_1 Q^2}\,, \qquad (22)$$

or

$$T_2 = \frac{1}{\mathbf{k}_\perp^2 - d_2(\bar{x}\pm\xi)Q^2 - \mathrm{i}\varepsilon}\,, \qquad (23)$$

where $d_i \geq 0$. The Fourier transforms of these propagator terms can readily be obtained:

$$\begin{aligned}\hat{T}_1 &= \frac{1}{2\pi}K_0(\sqrt{d_1}\,bQ)\,,\\ \hat{T}_2 &= \frac{1}{2\pi}K_0\left(\sqrt{d_2(\pm\xi-\bar{x})}\,bQ\right)\theta(\pm\xi-\bar{x})\\ &\quad + \frac{\mathrm{i}}{4}H_0^{(1)}\left(\sqrt{d_2(\bar{x}\pm\xi)}bQ\right)\theta(\bar{x}\pm\xi)\,, \qquad (24)\end{aligned}$$

[1] For the quark subprocess the trace includes the hadronic matrix element that defines the GPDs and is $\propto \gamma^+$ or $\propto \gamma^+\gamma_5$.

[2] Note that for longitudinally polarized vector mesons $\epsilon(0) \simeq q'/m_V$. Hence, the spin wave function is $\propto \not{q}'$ in this case up to mass corrections. A mass term $\propto m_V \not{\epsilon}_V$ in the spin wave function for transversely polarized vector mesons has been investigated [4, 5]. In collinear approximation this term leads to an infrared singular twist-3 contribution. Such mass terms are neglected by us.

[3] All its elements are zero except $g_\perp^{11} = g_\perp^{22} = -1$.

where K_0 and $H_0^{(1)}$ are the zeroth order modified Bessel function of the second kind and the Hankel function, respectively.

3 The double distribution model

As in [1, 3] the GPDs are constructed from the PDFs with the help of double distributions [7, 8]. Since this construction is described in detail in our previous papers we will only recapitulate a few basic elements of it [1, 3]. The main advantage of this construction is the warranted polynomiality of the resulting GPDs and the correct forward limit $\xi, t \to 0$. It is well known that, at low x, the parton distribution functions behave as powers δ_i of x. These powers are assumed to be generated by Regge poles [21, 22]. We generalize this behavior of the PDFs by assuming that the t dependence of the double distributions and hence the GPDs are also under control of Regge behavior. Linear Regge trajectories are assumed for small $-t$:

$$\alpha_i = \alpha_i(0) + \alpha_i' t\,, \quad i = g, \mathrm{sea}, \mathrm{val}\,, \tag{25}$$

with $\delta_i = \alpha_i(0)$ for quarks and, as a consequence of the familiar definition of the gluon GPD, which reduces to $\bar{x}g(\bar{x})$ in the forward limit, $\delta_g = \alpha_g(0) - 1$ for gluons. The trajectories are accompanied by Regge residues assumed to have an exponential t dependence with parameters b_i. The following ansatz for the double distributions associated with the GPDs H_i is therefore employed [3]:

$$f_i(\beta,\alpha,t) = \mathrm{e}^{b_i t} \mid \beta \mid^{-\alpha_i' t} h_i(\beta) \times \frac{\Gamma(2n_i+2)}{2^{2n_i+1}\Gamma^2(n_i+1)} \frac{[(1-|\beta|)^2-\alpha^2]^{n_i}}{(1-|\beta|)^{2n_i+1}}\,, \tag{26}$$

where

$$\begin{aligned} h_g(\beta) &= |\beta| g(|\beta|)\,, & n_g &= 2\,,\\ h^q_{\mathrm{sea}}(\beta) &= q_{\mathrm{sea}} w(|\beta|)\mathrm{sign}(\beta)\,, & n_{\mathrm{sea}} &= 2\,,\\ h^q_{\mathrm{val}}(\beta) &= q_{\mathrm{val}}(\beta)\Theta(\beta)\,, & n_{\mathrm{val}} &= 1\,. \end{aligned} \tag{27}$$

For the decomposition of the double distribution into a valence and a sea contribution we follow the procedure proposed in [12] and write

$$\begin{aligned} f^q_{\mathrm{val}}(\beta,\alpha,t) &= \big[f^q(\beta,\alpha,t) + f^q(-\beta,\alpha,t)\big]\Theta(\beta)\,,\\ f^q_{\mathrm{sea}}(\beta,\alpha,t) &= f^q(\beta,\alpha,t)\Theta(\beta) - f^q(-\beta,\alpha,t)\Theta(-\beta)\,. \end{aligned} \tag{28}$$

In the forward limit, $\xi, t \to 0$, this decomposition is conform the usual definition of sea- and valence-quark PDFs.

The GPDs are related to the double distributions by the integral

$$H_i(\bar{x},\xi,t) = \int_{-1}^{1} \mathrm{d}\beta \int_{-1+|\beta|}^{1-|\beta|} \mathrm{d}\alpha\, \delta(\beta+\xi\alpha-\bar{x}) f_i(\beta,\alpha,t)\,. \tag{29}$$

For convenience we employ an expansion of the PDFs ($\beta > 0$)

$$h_i(\beta) = \beta^{-\delta_i}(1-\beta)^{2n_i+1} \sum_{j=0}^{3} c_{ij}\beta^{j/2}\,, \tag{30}$$

which is particularly useful at low β and allows us to perform the integral (29) term by term analytically; its use is also convenient if the integral (29) is carried out numerically. The factor $(1-\beta)^{2n_i+1}$ serves for canceling the corresponding factor in (26) and has the additional welcome feature of roughly accounting for the $\beta \to 1$ behavior of the PDFs. The ansatz (30) results in a corresponding expansion of the GPDs

$$H_i(\bar{x},\xi,t) = \mathrm{e}^{b_i t} \sum_{j=0}^{3} c_{ij} H_{ij}(\bar{x},\xi,t)\,. \tag{31}$$

The definition of the GPDs is completed by the relations

$$\begin{aligned} H^g(-\bar{x},\xi,t) &= H^g(\bar{x},\xi,t)\,,\\ H^q_{\mathrm{sea}}(-\bar{x},\xi,t) &= -H^q_{\mathrm{sea}}(\bar{x},\xi,t)\,, \end{aligned} \tag{32}$$

and

$$H^q_{\mathrm{val}}(\bar{x},\xi,t) = 0\,, \quad -1 \le \bar{x} < -\xi\,. \tag{33}$$

In (29) the so-called D terms for the gluons and the flavor singlet quark combination are ignored [23]. The D terms ensure the appearance of the highest powers of the skewness in the moments of the GPDs. They only contribute to the less important real parts of the amplitudes since their support is the region $-\xi < x < \xi$. The corresponding imaginary parts are related to the GPDs at $\bar{x} = \xi(1 + 2\mathbf{k}_\perp^2/(\tau Q^2))$, which lies outside the support of the D terms. We take this in vindication of neglecting the D terms.

For the expansions of the PDFs we will use the same parameters as in [3] with the exception of a little change. ZEUS [24] now provides data on the cross section for ρ production up to $Q^2 = 100\,\mathrm{GeV}^2$, whereas in [3] the fits to the CTEQ6M PDFs were made for $Q^2 \le 40\,\mathrm{GeV}^2$. As one may check, the CTEQ6M gluon and sea-quark PDFs are not well described above $40\,\mathrm{GeV}^2$ by the expansion quoted in [3], but the addition of a L^2 term to δ_g,

$$\delta_g = 0.10 + 0.06L - 0.0027L^2\,, \tag{34}$$

improves the fits to the gluon and sea-quark PDFs considerably, as can be seen from Fig. 2 ($L = \ln Q^2/Q_0^2$ and $Q_0^2 = 4\,\mathrm{GeV}^2$). The L^2 term is irrelevant below $40\,\mathrm{GeV}^2$. The valence quarks are not needed at high Q^2. The parameters of the expansions (30) are quoted in Table 1. We stress that with the exception of δ_g, they are identical to those used in [3]. In the quoted ranges of Q^2 and β the fits to the PDFs agree very well with the CTEQ6M solution; they are always well inside the band of Hessian errors quoted in [6]. Larger values of β are irrelevant to us, since the region $0.5 \lesssim \beta$ affects the real parts of the amplitudes only marginally; the contributions are less than 0.5%. From the fitted PDFs the GPDs are evaluated with the help of (29).

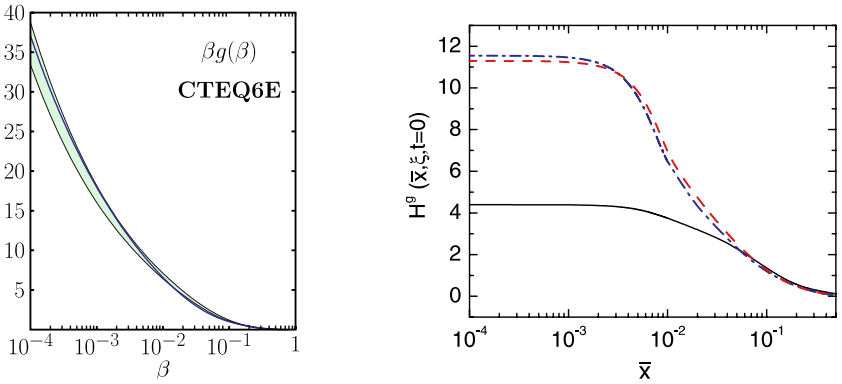

Fig. 2. *Left*: the CTEQ6 gluon PDF at $Q^2 = 100\,\mathrm{GeV}^2$ as compared to our fit (*solid line*). The *band* indicates the Hessian errors of the PDFs. *Right*: the gluon GPD H^q at $\xi = 0.01$ and $t = 0$. *Solid line*: H^g at the initial scale $4\,\mathrm{GeV}^2$. *Dash-dotted* (*dashed*) *line*: at the scale of $40\,\mathrm{GeV}^2$ evolved with the Vinnikov code [27] (approximate evolution)

Table 1. The parameters appearing in the expansion (30) of the PDFs ($L = \ln Q^2/Q_0^2$, $Q_0^2 = 4\,\mathrm{GeV}^2$)

	gluon	strange	u_{val}	d_{val}
δ	Eq. (34)	$1+\delta_g$	0.48	0.48
α'	$0.15\,\mathrm{GeV}^{-2}$	$0.15\,\mathrm{GeV}^{-2}$	$0.9\,\mathrm{GeV}^{-2}$	$0.9\,\mathrm{GeV}^{-2}$
c_0	$2.23+0.362L$	$0.123+0.0003L$	$1.52+0.248L$	$0.76+0.248L$
c_1	$5.43-7.00L$	$-0.327-0.004L$	$2.88-0.940L$	$3.11-1.36L$
c_2	$-34.0+22.5L$	$0.692-0.068L$	$-0.095L$	$-3.99+1.15L$
c_3	$40.6-21.6L$	$-0.486+0.038L$	0	0

In an attempt to keep the GPD model simple we assume

$$H^u_{\mathrm{sea}} = H^d_{\mathrm{sea}} = \kappa_s H^s_{\mathrm{sea}}\,, \tag{35}$$

where the flavor-symmetry breaking factor is parameterized as

$$\kappa_s = 1 + 0.68/(1 + 0.52\ln Q^2/Q_0^2)\,, \tag{36}$$

as obtained from a fit to the CTEQ6M PDFs.

As in [3] we take for the slope of the gluon trajectory the value $\alpha'_g = 0.15\,\mathrm{GeV}^{-2}$. Since the sea-quark PDFs are mainly driven by evolution for $Q^2 \gtrsim 4\,\mathrm{GeV}^2$ it is assumed that $\alpha_{\mathrm{sea}}(t) = \alpha_g(t)$. A standard trajectory is adopted for the valence-quark Regge pole – $\alpha_{\mathrm{val}}(t) = 0.48 + 0.9\,\mathrm{GeV}^{-2}\,t$. The parameter of the gluon residue is fixed from a fit against the HERA data for ρ [25] and ϕ production [26]:

$$b_g = b_{\mathrm{sea}} = 2.58\,\mathrm{GeV}^{-2} + 0.25\,\mathrm{GeV}^{-2}\ln\frac{m^2}{Q^2+m^2}\,, \tag{37}$$

The ρ and ϕ slopes of the cross sections practically overlap at HERA energies; there are only minor differences at low Q^2. The parameter b_g given in (37) leads to a t dependence of the differential cross section in perfect agreement with the recent ZEUS data [24]. The parameter of the valence-quark residue is taken to be zero. This is in accord with the findings of the nucleon form factor analysis proposed in [9], in which the zero-skewness GPDs have been determined.

We emphasize that the evolution of the GPDs is taken into account by us only approximately through the evolution of the PDFs. This is reasonable, since at low ξ the imaginary part of the gluon (and sea quark) contribution dominates, which is $\propto H^g(\xi,\xi,t)$ and therefore approximately equals $2\xi g(2\xi)$ at low ξ (see, for instance [1]). Its real part as well as the valence quark contributions are only of importance near $4\,\mathrm{GeV}^2$, the initial value of the evolution. The very time-consuming numerical integration on $x, \mathbf{b}$ and τ forces us to use this approximative treatment of the evolution. In order to demonstrate the quality of our approximation we compare in Fig. 2 the gluon GPD at $40\,\mathrm{GeV}^2$ either obtained from our approximation or from evolving H^g from the initial scale of $4\,\mathrm{GeV}^2$ using the evolution code developed by Vinnikov [27]. Only minor differences are to be noticed.

4 Results on cross sections

Before we present our results obtained from the handbag approach we have to specify the meson wave functions used in the evaluation of the amplitudes. As in [1, 3] we will take Gaussian wave functions ($j = \mathrm{L}, \mathrm{T}$)

$$\begin{aligned}\Psi_{Vj}(\tau,\mathbf{k}_\perp) = {} & 8\pi^2\sqrt{2N_c}f_{Vj}(\mu_{\mathrm{F}})a_{Vj}^2 \\ & \times\left[1 + B_2^{Vj}(\mu_{\mathrm{F}})C_2^{3/2}(2\tau-1)\right] \\ & \times\exp\left[-a_{Vj}^2\mathbf{k}_\perp^2/(\tau\bar\tau)\right].\end{aligned} \tag{38}$$

Transverse momentum integration leads to the meson distribution amplitudes for which we allow for the second Gegenbauer moment besides the asymptotic form. The meson decay constants for longitudinally polarized vector mesons are known from the electronic decays of the vector

mesons, while those for transversely polarized mesons are taken from QCD sum rules [28]. In contrast to the decay constants $f_{V\mathrm{L}}$ the latter ones are scale dependent:

$$f_{V\mathrm{T}}(\mu_\mathrm{F}) = f_{V\mathrm{T}}(\mu_0)\left(\frac{\alpha_\mathrm{s}(\mu_\mathrm{F})}{\alpha_\mathrm{s}(\mu_0)}\right)^{4/27} . \tag{39}$$

Note that the decay constants for transversely polarized vector mesons always appear in the combination $f_{V\mathrm{T}}/M_V$, i.e. there is only one independent parameter in practice. In fact we use a typical constituent mass of 300 MeV for M_V and the QCD sum rule result [28] $f_{V\mathrm{T}}/f_{V\mathrm{L}} \simeq 0.8$ at the scale of $\mu_0 = 1$ GeV. The Gegenbauer coefficients $B_2^{V\mathrm{L}}$ have been found to be zero in the analysis of the longitudinal cross section [3]. Those for the transverse case are fitted to the data on the σ_T or the cross section ratio $R = \sigma_\mathrm{L}/\sigma_\mathrm{T}$. The Gegenbauer coefficients are scale dependent:

$$B_2^{Vj}(\mu_\mathrm{F}) = B_2^{Vj}(\mu_0)\left(\frac{\alpha_\mathrm{s}(\mu_\mathrm{F})}{\alpha_\mathrm{s}(\mu_0)}\right)^{\gamma_{2j}} , \tag{40}$$

where $\gamma_{2\mathrm{L}} = 50/81$ and $\gamma_{2\mathrm{T}} = 40/81$ [29]. Finally, the transverse size parameters a_{Vj} in (38) are either fitted to σ_L or to σ_T depending on the polarization of the vector meson. The values for the various parameters are compiled in Table 2. Those for the longitudinal case are identical to the parameters used in [3].

The assessment of the theoretical uncertainties deserves special considerations. The results on the cross sections (and other observables) are subject to parametric errors. The main uncertainties stem from the Hessian errors of the set of CTEQ6 PDFs. Since for the longitudinal cross section the parameters of the corresponding wave functions are adjusted so that good agreement between the data on σ_L and the handbag results is achieved, there are no substantial additional uncertainties from the longitudinal wave function. Results for σ_L evaluated from sets of PDFs other than CTEQ6 also fall into the error bands in most cases (an exception is set for instance by the PDFs determined in [30, 31]) provided these PDFs are treated in analogy to the CTEQ6M set, i.e. they are fitted to the expansion (30) by forcing them to behave Regge-like with powers δ_i as described above, and, if necessary, readjusting the transverse size parameters. The uncertainties in the ratio, R, of the longitudinal and transverse cross sections mainly arise from the uncertainties of the wave functions for transversely polarized vector mesons (i.e. from the Gegenbauer coefficients, the transverse size parameters and from the ratio $f_{V\mathrm{T}}/M_V$). The errors due to those of the GPDs or PDFs, which are mainly responsible for the theoretical uncertainties of the cross sections, cancel to a large extent in the ratio.

Table 2. The parameters appearing in the wave function (38), quoted at the scale $\mu_0 = 1$ GeV

parameter	ϱ_L	ϱ_T	φ_L	φ_T
f_V [MeV]	209	167	221	177
a_V [GeV^{-1}]	0.75	1.0	0.70	0.95
B_2^V	0.0	0.10	0.0	0.10

The results for the longitudinal cross sections are the same as in [3]. We refrain from showing them again. The experimental data on the cross section ratio R are customarily determined from the measured SDME r_{00}^{04} by the relation

$$R = \frac{\sigma_\mathrm{L}}{\sigma_\mathrm{T}} = \frac{1}{\varepsilon}\frac{r_{00}^{04}}{1 - r_{00}^{04}} . \tag{41}$$

The SDME in (41) is understood to be integrated over the full range of t available in a given experiment.[4] The theoretical and experimental results on the ratio R are compared in Figs. 3 and 4. In general we achieve very good agreement with experiment, in particular with regard to the theoretical uncertainties displayed as shaded bands in the plots.

The ratio R is mildly energy dependent for W larger than about 10 GeV, while, for lower energies, it exhibits a somewhat stronger energy dependence, in particular at larger values of Q^2; see Fig. 4. This implies differences in the energy dependences of σ_L and σ_T, which can be traced back to the different hard scattering kernels (see e.g. (19)) and the varying wave functions for longitudinally and transversely polarized vector mesons, in particular to the different values of the r.m.s. $\mathbf{k}_\perp$ ($\sim 1/a_V$). An energy dependence of R seems to be indicated by the preliminary HERMES [35, 36] and COMPASS [38] data although confirmation of this observation is demanded. Most of the older experiments have rather large errors, so that a definite conclusion on a possible W dependence cannot be drawn at present. Unfortunately, for ϕ production there is only one low energy data point available [37] and this point is measured at the very low value of $Q^2 = 2.6$ GeV^2, which lies outside the range where the handbag approach, in its present form, can be trusted. We note that for ϕ production the energy dependence of R is even milder than for the case of the ρ; the results for $W = 10$ GeV practically fall together with those at 75 GeV.

In Fig. 5 the handbag results on the ρ and ϕ cross sections are compared to experiment. Again good agreement with the H1 [25, 32] and ZEUS [24, 26, 34] data is observed in a large range of Q^2. The leading-twist contribution to these cross sections, i.e. σ_L evaluated in collinear approximation, is also shown. Although the leading-twist contribution approaches the experimental cross section with increasing Q^2 there is still a small difference of about 1.5σ between both at $Q^2 = 100\,\mathrm{GeV}^2$ for ρ production. Note that even at that value of Q^2 the transverse cross section, which is included in the full one and also represents a power correction to the leading-twist result, is not negligible; it amounts to about 10%. The leading-twist contribution is about 20% larger than the one obtained within the modified perturbative approach at $Q^2 = 100\,\mathrm{GeV}^2$, i.e. the corrections due the quark transverse momentum have not yet disappeared completely. In Fig. 6 the energy dependence of

[4] The cross sections σ_L and σ_T have been obtained from integrating the differential cross sections over that range of t.

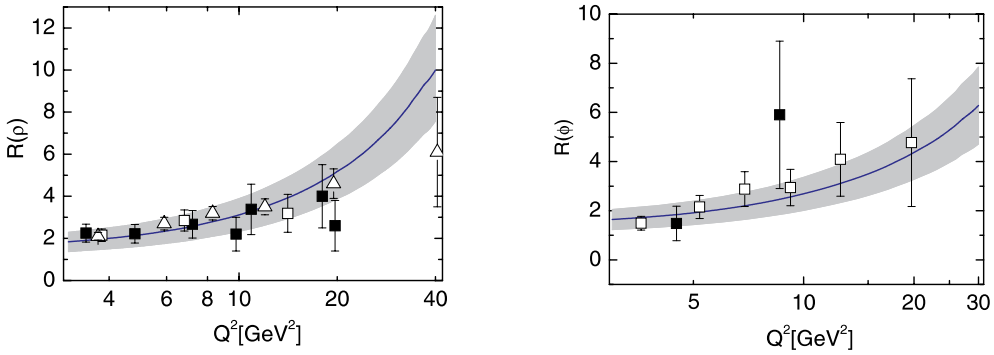

Fig. 3. The ratio of longitudinal and transverse cross sections for ϱ (*left*) and φ (*right*) production versus Q^2 at $W = 90$ GeV and 75 GeV, respectively. The data are taken from H1 [25, 32, 33] (*solid squares*) and ZEUS [26, 34] (*open squares*), respectively. The recent ZEUS data [24] are shown as *open triangles*. The *solid lines* represent the handbag results with the *shaded bands* indicating the uncertainties of the predictions

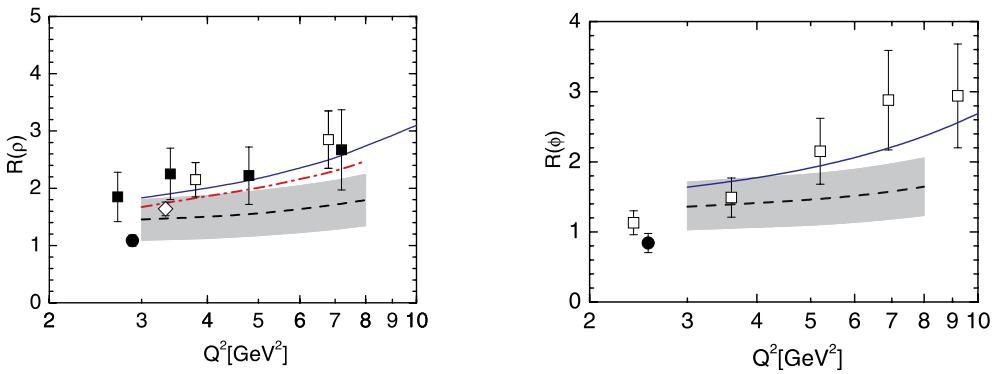

Fig. 4. Handbag results for R on ϱ (*left*) and φ (*right*) production at $W = 75\,(10\,, 5)$ GeV shown as *solid* (*dash-dotted, dashed*) *line*. The data are taken from [25, 26, 34]. Preliminary data from HERMES [35–37] (*solid circle*) and COMPASS [38] (*diamond*). The *error bands* are only shown at $W = 5$ GeV. For further notation refer to Fig. 3

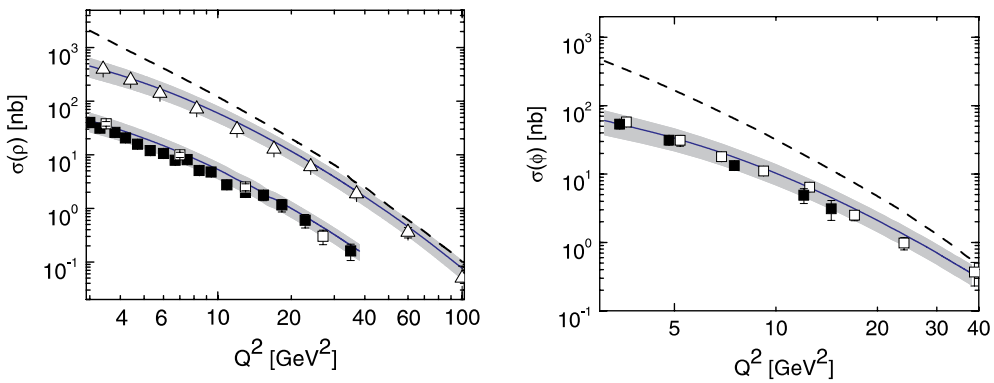

Fig. 5. The Q^2-dependence of the cross sections for ϱ (*left*) and φ (*right*) production at $W = 90$ (ϱ) and 75 GeV (ϱ, φ). The data are taken from ZEUS [24, 26, 34] and H1 [25, 32]. For ϱ production at $W = 75$ GeV the data and theoretical results are divided by 10 for ease of legibility. The *dashed lines* represent the leading-twist contribution. For further notation refer to Fig. 3

the ρ cross section at a set of Q^2 values is displayed. Within errors agreement is seen with the ZEUS data [24]. This is not a surprise, since the power δ_g, related to the intercept of the gluonic Regge intercept, is fixed by the energy dependence of the HERA data on the cross sections [3]. As is $\sigma_{\rm L}$ [3], the full cross section at HERA energies is dominated by the gluon contribution, although the sea quarks are not negligible. Including the interference with the gluon the sea quarks contribute about 25% in the case of the ϕ and 40% in the case of the ρ at $Q^2 = 4\,\text{GeV}^2$. The larger sea-quark contribution in the latter case is due to the flavor-symmetry breaking factor κ_s (36). Flavor symmetry breaking in the sea is important for the ratio of the ϕ and ρ cross sections [3]. Neglecting the sea quarks or

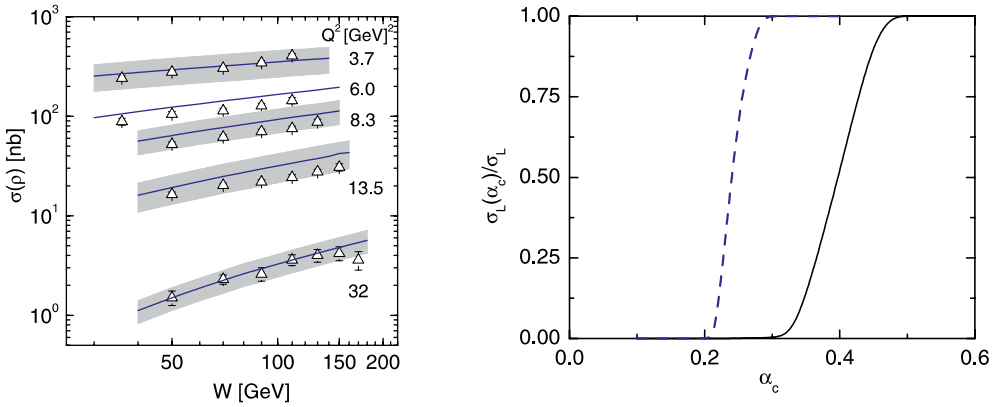

Fig. 6. *Left*: the cross section for ϱ production versus W at a set of Q^2 values. The data are taken from ZEUS [24]. For further notation refer to Fig. 3. The *error band* at 6 GeV^2 is omitted for ease of legibility. *Right*: the accumulation profile of the amplitude in dependence of $\alpha_c^{\rm crit}$ at $Q^2 = 4$ (*solid line*) and 40 GeV^2 (*dashed line*) at $W = 75$ GeV

assuming a flavor symmetric sea leads to an incorrect ϕ–ρ ratio. Going to energies lower than about 10 GeV the valence quark contributions gradually become perceptible for ρ production. At, say, 5 GeV the valence quarks are responsible for about 40% of the cross section. We stress that the three contributions have to be added coherently. There are substantial interference terms, which increase the cross sections markedly. For instance, at $W = 5$ GeV and $Q^2 = 4$ GeV^2, the ρ cross section is doubled by the interference terms.

A remark concerning the t dependence of the differential cross sections is in order. As we pointed out in [3], the cross sections drop exponentially with t to a very good approximation. Their slopes are approximately given by $2b_g$ (see (37)) plus a contribution from the gluonic Regge trajectory (see (26) and [3]). At large W the slopes of the differential cross sections for longitudinally and transversely polarized photons are the same, while, at low W, the valence quarks generate small differences. Consequently, the ratio R is nearly t independent – a fact that is in agreement with the ZEUS measurement [24].

Finally, we check the theoretical consistency of the modified perturbative approach. Consistency is meant in the sense that the bulk of the perturbative contributions should be accumulated in regions where the strong coupling α_s is sufficiently small. To find out whether or not this is the case, we set the integrand in (11) equal to zero in those regions where $\alpha_s(\mu_R) > \alpha_s^{\rm crit}$, and evaluate, say, the longitudinal cross section for ρ production as a function of $\alpha_s^{\rm crit}$. Consulting Fig. 6, where the accumulation profile is shown, one observes that almost the entire result is accumulated in a comparatively narrow region of α_s around 0.4 at $Q^2 = 4$ GeV^2 and 0.25 at 40 GeV^2. Thus the effective renormalization scales in these two cases are about 1.5 and 15 GeV^2, respectively. Hence, our results on the cross sections are theoretically self-consistent with regard to the above-mentioned criterion. Contributions from the endpoint regions where the momentum fraction τ tends either to zero or to one and where, in collinear approximation, the renormalization scale becomes very small, are sufficiently suppressed.

5 Results on spin density matrix elements

In a number of experiments [24, 25, 32, 38, 39] the SDMEs have been extracted from the measured decay angular distributions of the vector mesons. The formalism of the SDMEs, i.e. their relations to the amplitudes for the process $\gamma^* p \to V p$, has been developed by Schilling and Wolf [40] a long time ago. This work has recently been repeated and extended to the case of a transversely polarized target proton by Diehl [41]. Since in the experimental papers the notation of [40] is used throughout, we will adhere to it here in order to facilitate comparison.

The SDMEs are given by properly normalized bilinear combinations of $\gamma^* p \to V p$ amplitudes. Due to the symmetry relations (9) and (10) there are no interference terms between $\mathcal{M}^N$ and $\mathcal{M}^U$ in the case of unpolarized electroproduction of vector mesons. The normalizations read

$$N_{\rm L} = 2 \sum_{\nu'} |\, \mathcal{M}^N_{0\nu',0+} \,|^2 \,,$$
$$N_{\rm T} = 2 \sum_{\nu'} \left[|\, \mathcal{M}^N_{+\nu',++} \,|^2 + |\, \mathcal{M}^U_{+\nu',++} \,|^2 \right] , \qquad (42)$$

where helicity-flip $\gamma^* \to V$ transitions are neglected, as we do throughout this work. Up to a phase space factor, see (7), the normalizations are the differential cross sections for longitudinally and transversely polarized vector mesons. Since the SDMEs also provide a possibility to study the role of $\widetilde{H}$, we do not ignore the contributions from the corresponding amplitude $\mathcal{M}^U_{+\nu',++}$ in (42) for later reference.

Obviously, the SDMEs are functions of Q^2, t and W. Due to limitations in statistics it is not possible to measure the SDMEs as functions of the three variables. Thus, frequently the SDMEs are presented as functions of one variable for average values of the other variables. For instance, the SDMEs are quoted as a function of Q^2 for an average value of W and integrated over all t available in a given experiment. Only in this case, and this is an important one to which we will mainly refer in the following,

the normalizations $N_{\rm L}$ and $N_{\rm T}$ refer to the respective integrated cross sections $\sigma_{\rm L}$ and $\sigma_{\rm T}$ up to the phase-space factor and eventually neglected suppressed amplitudes. If for instance the SDMEs are presented as a function of t the normalization represents differential cross sections at a fixed value of t but integrated over certain ranges of Q^2 and W.

The SDMEs allow for a separation of the absolute values of the two amplitudes, $\mathcal{M}^N_{0+,0+}$ and $\mathcal{M}^N_{++,++}$, and for a test of their relative phases. Whether or not it is justified to neglect the other amplitudes can be examined as well. The SDMEs r^{04}_{00}, r^1_{1-1} and $\mathrm{Im}\, r^2_{1-1}$ are related to the cross section ratio R. In terms of the amplitudes we are investigating these SDMEs read

$$\begin{aligned} r^{04}_{00} &= \frac{2\varepsilon}{N_{\rm T}+\varepsilon N_{\rm L}} \sum_{\nu'} |\, \mathcal{M}^N_{0\nu',0+}\,|^2\,, \\ r^1_{1-1} &= -\mathrm{Im}\, r^2_{1-1} \\ &= \frac{1}{N_{\rm T}+\varepsilon N_{\rm L}} \sum_{\nu'} \Big[|\, \mathcal{M}^N_{+\nu',++}\,|^2 - |\, \mathcal{M}^U_{+\nu',++}\,|^2 \Big]\,. \end{aligned} \tag{43}$$

Neglecting the amplitude $\mathcal{M}^U$ too, these expressions simplify to

$$1 - r^{04}_{00} = 2r^1_{1-1} = -2\mathrm{Im}\, r^2_{1-1} = \frac{1}{1+\varepsilon R}\,. \tag{44}$$

In Figs. 7–9 this prediction of our handbag approach is compared to experiment. The agreement is in general good within errors although with occasional exceptions. Thus, for ρ production, r^1_{1-1} and $\mathrm{Im}\, r^2_{1-1}$ are not perfectly reproduced. On the other hand, their sum, measuring the double flip transitions $\gamma^*_{\rm T} \to V_{-\rm T}$, is nicely in agreement with zero. A further check is provided by the t dependence of the SDMEs. Since in the handbag approach the t dependence solely comes from the GPDs and these are identical for the two amplitudes, the above SDMEs should be nearly flat in t, which is indeed the case experimentally within errors [24, 25]. Hence, the above three SDMEs are consistent with our assumptions and do not provide a significant signal for helicity-flip amplitudes or contributions from $\widetilde{H}$. The W dependence of the handbag predictions is displayed in Fig. 8. It is evidently very mild. In particular the results for the SDMEs at $W = 75$ and 90 GeV fall practically together.

After having checked that the absolute values of our two amplitudes are in fair agreement with experiment, we now turn to their relative phase $\delta_{\rm LT}$. In terms of our two amplitudes, the SDMEs relevant for the verification of the phase read

$$\begin{aligned} \mathrm{Re}\, r^5_{10} = -\mathrm{Im}\, r^6_{10} &= \frac{1}{\sqrt{2}} \frac{1}{N_{\rm T}+\varepsilon N_{\rm L}} \mathrm{Re}\, \big[\mathcal{M}^N_{++,++} \mathcal{M}^{N*}_{0+,0+}\big] \\ &= \frac{1}{2\sqrt{2}} \frac{\sqrt{R}}{1+\varepsilon R} \cos\delta_{\rm LT}\,. \end{aligned} \tag{45}$$

The predictions for the SDMEs in the case of ϕ production are shown in Figs. 9 and 10. Fair agreement with experiments can be seen. For ρ production, on the other hand, a conflict is to be noted; see Figs. 7 and 8. The data [24, 25, 35, 36] require a rather large phase although with strong fluctuations (10–30°), while the handbag approach provides only a small value for it (e.g. $\delta_{\rm LT} = 3.1°$ at $W = 5$ GeV and $Q^2 = 3\,\mathrm{GeV}^2$). Whether our model for the $\gamma^*_{\rm T} \to V_{\rm T}$ amplitude, which represents a power correction to the leading $\gamma^*_{\rm L} \to V_{\rm L}$ amplitude, is inadequate for this detail needs further investigation. However, that the sum $\mathrm{Re}\, r^5_{10} + \mathrm{Im}\, r^6_{10}$ amounts to only 1% of the corresponding difference of these SDME makes it clear that the neglected helicity-flip $\gamma^* \to V$ transitions in (45) are not responsible for the observed conflict.

The HERMES collaboration has also measured the angular distribution of the decay of the ρ in the case of a longitudinally polarized lepton beam. These measurements, which have not yet been analyzed, will provide data on other SDMEs [40]. For instance, the SDMEs $\mathrm{Im}\, r^7_{10}$ and

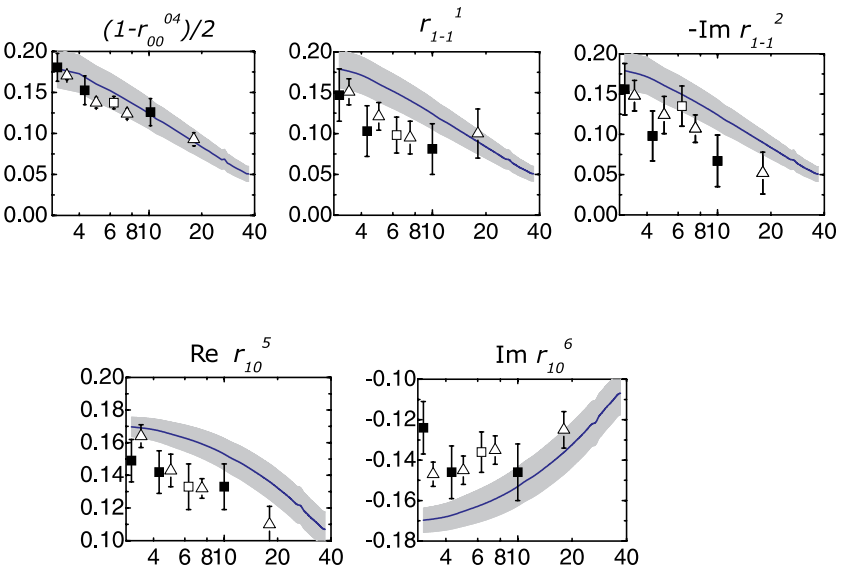

Fig. 7. The SDMEs for the ϱ meson versus Q^2 (in GeV^2) at $W = 75$ GeV. The data are taken from [24, 25, 39]. Note the different scales at the axis of ordinates. For further notation refer to Fig. 3

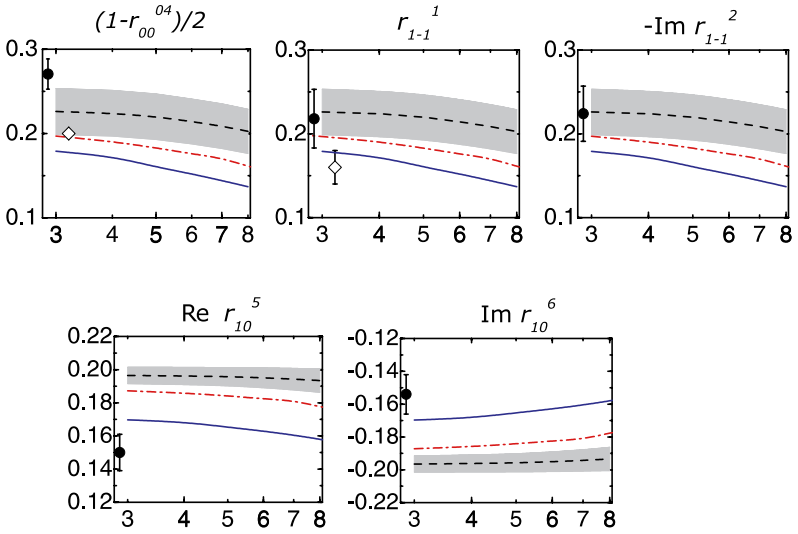

Fig. 8. SDMEs for the ϱ meson versus Q^2 (in GeV^2) at $W = 5, 10$ and 75 GeV (*dashed, dash-dotted and solid line*, respectively). Preliminary data taken from HERMES [35, 36] (*solid circles*) and COMPASS [38] (*diamonds*). *Error bands* are only shown for $W = 5$ GeV. For further notation refer to Figs. 3 and 4

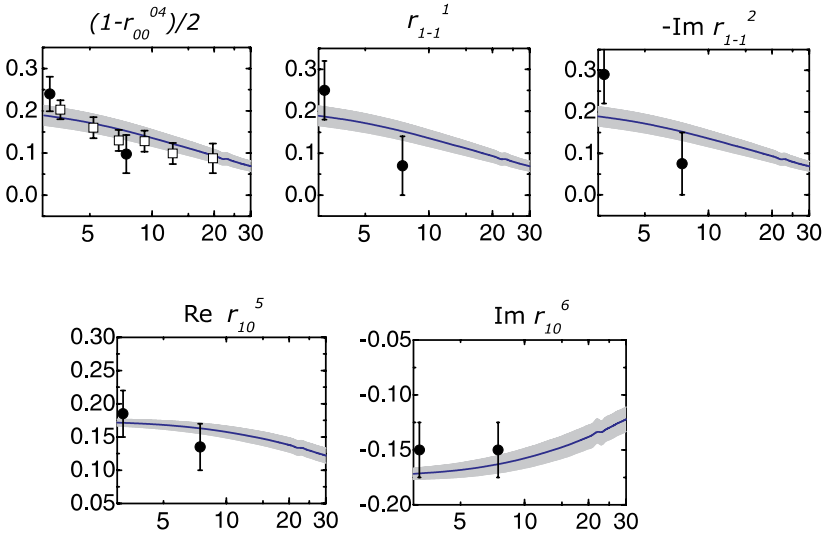

Fig. 9. SDMEs for the φ meson versus Q^2 (in GeV^2) at $W = 75$ GeV. The data are taken from [26, 32]. For further notation refer to Fig. 3

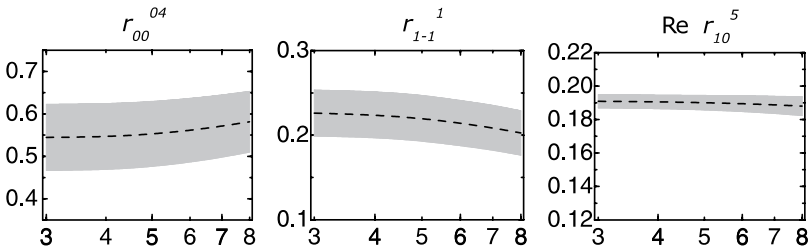

Fig. 10. SDMEs for the φ meson versus Q^2 (in GeV^2) at $W = 5$ GeV

$\mathrm{Re}\, r^8_{10}$ also measure the phase δ_{LT} introduced in (45):

$$\mathrm{Im}\, r^7_{10} = \mathrm{Re}\, r^8_{10} = \frac{1}{2\sqrt{2}} \frac{\sqrt{R}}{1+\varepsilon R} \sin\delta_{\mathrm{LT}}\,. \qquad (46)$$

Predictions for these SDMEs are shown in Fig. 11. The other polarized SDMEs are only sensitive to the suppressed amplitudes; see Table 3.

In principle also the helicity-flip $\gamma^* \to V$ transitions can be calculated in the proposed handbag approach as well. But these transitions are strongly suppressed with respect to the amplitude $\mathcal{M}_{0+,0+}$ as the amplitude for $\gamma^*_{\mathrm{T}} \to V_{\mathrm{T}}$ transitions; see (18). In fact,

$$\gamma^*_{\mathrm{T}} \to V_{\mathrm{L}} \propto \frac{\sqrt{-t}}{Q}\,,$$

$$\gamma^*_{\mathrm{L}} \to V_{\mathrm{T}} \propto \frac{\sqrt{-t}\langle \mathbf{k}^2_\perp \rangle^{1/2}}{Q^2}\,,$$

$$\gamma^*_{\mathrm{T}} \to V_{-\mathrm{T}} \propto \frac{-t\,\langle \mathbf{k}^2_\perp \rangle^{1/2}}{Q^3}\,, \qquad (47)$$

Table 3. SDMEs controlled by helicity-flip $\gamma^* \to V$ transitions

SDME	amplitudes	order
r^5_{00}, r^8_{00}	$(\gamma^*_{\rm T} \to V_{\rm L})(\gamma^*_{\rm L} \to V_{\rm L})$	$\sqrt{-t}/Q$
$\mathrm{Re}\, r^{04}_{10}$, $\mathrm{Re}\, r^1_{10}$, $\mathrm{Im}\, r^2_{10}$, $\mathrm{Im}\, r^3_{10}$	$(\gamma^*_{\rm T} \to V_{\rm L})(\gamma^*_{\rm T} \to V_{\rm T})$	$\sqrt{-t}\langle \mathbf{k}^2_\perp\rangle^{1/2}/Q^2$
r^1_{00}	$\mid(\gamma^*_{\rm T} \to V_{\rm L})\mid^2$	$-t/Q^2$
$r^5_{11}, r^5_{1-1}, \mathrm{Im}\, r^6_{1-1}$	$(\gamma^*_{\rm L} \to V_{\rm T})(\gamma^*_{\rm T} \to V_{\rm T})$	$\sqrt{-t}\langle \mathbf{k}^2_\perp\rangle/Q^3$
$r^8_{11}, r^8_{1-1}, \mathrm{Im}\, r^7_{1-1}$	$(\gamma^*_{\rm L} \to V_{\rm T})(\gamma^*_{\rm T} \to V_{\rm T})$	$\sqrt{-t}\langle \mathbf{k}^2_\perp\rangle/Q^3$
r^{04}_{1-1}, r^1_{11}, $\mathrm{Im}\, r^3_{1-1}$	$(\gamma^*_{\rm T} \to V_{-\rm T})(\gamma^*_{\rm T} \to V_{\rm T})$	$-t\langle \mathbf{k}^2_\perp\rangle/Q^4$

where the powers of $\sqrt{-t}/Q$ follow from angular momentum conservation and the factors $\langle \mathbf{k}^2_\perp\rangle^{1/2}/Q$ are from the treatment of transversely polarized vector meson; see (18). The suppression factors given in (47) engender the behavior of the SDMEs for the helicity-flip $\gamma^* \to V$ transitions listed in Table 3. The most important helicity-flip amplitude is the one for $\gamma^*_{\rm T} \to V_{\rm L}$ transitions. It is most clearly seen in r^5_{00} as an interference term with the dominant longitudinal amplitude. It is definitely non-zero, being of the order of 0.1 for ρ and ϕ production in experiment [24, 25, 35, 36]. At least HERMES [35, 36] observes a t dependence for it in agreement with expectation ($\propto \sqrt{-t}$). The contribution of the $\gamma^*_{\rm T} \to V_{\rm L}$ amplitude to the cross sections, R and r^{04}_{00}, is at the percent level and can safely be neglected. The other SDMEs related to the $\gamma^*_{\rm T} \to V_{\rm L}$ transitions are experimentally compatible with zero within errors. The only exception is to be seen in the recent high statistics ZEUS data [24], where $\mathrm{Im}\, r^2_{10}$ and $\mathrm{Re}\, r^1_{10}$ have very small but non-zero for values of Q^2 less than $10\,\mathrm{GeV}^2$. It would be interesting to see whether their t dependencies are in agreement with expectation. For the remaining SDMEs, being related to the $\gamma^*_{\rm L} \to V_{\rm T}$ and $\gamma^*_{\rm T} \to V_{-\rm T}$ transitions, there is no significant deviation from zero at large Q^2 experimentally. In view of these remarks it is fair to conclude that the neglect of the helicity-flip $\gamma^* \to V$ transitions in the cross sections for $Q^2 \geq 3\,\mathrm{GeV}^2$ is justified.

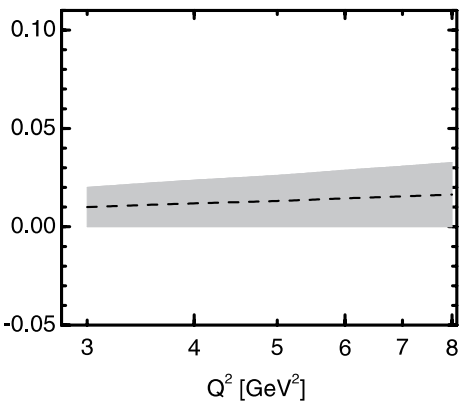

Fig. 11. The SDMEs $\mathrm{Im}\, r^7_{10}$ and $\mathrm{Re}\, r^8_{10}$ for ϱ production versus Q^2 at $W = 5\,\mathrm{GeV}$. The data are taken from [35, 36]; *solid* (*open*) *circle* is for $\mathrm{Im}\, r^7_{10}$ ($\mathrm{Re}\, r^8_{10}$). For further notation refer to Fig. 3

6 The role of $\widetilde{H}$

The expression for the amplitude $\mathcal{M}^U$ is the same as that for $\mathcal{M}^N$ given in (3), except that the sum of the subprocess amplitudes is to be replaced by their difference:

$$\mathcal{M}^{Ui}_{\mu+,\mu+}(V) = \frac{e}{2}\sum_a e_a \mathcal{C}^{\rm a}_V \times \int_{\bar{x}_i}^1 \mathrm{d}\bar{x}\left[\mathcal{H}^{Vi}_{\mu+,\mu+} - \mathcal{H}^{Vi}_{\mu-,\mu-}\right]\widetilde{H}^i(\bar{x},\xi,t)\,. \tag{48}$$

The superposition of the various quark and gluon contributions is identical to that for the amplitude $\mathcal{M}^N$. The unnatural parity amplitudes satisfy the symmetry relation (10). It is evident from (48) that parity conservation leads to a vanishing longitudinal amplitude $\mathcal{M}^U_{0+,0+}$. The transverse subprocess amplitude is the same as in (17) and (19), except that in the latter equation a plus sign occurs between $T_s T_a$ and $T_u T_b$ now.

The GPDs $\widetilde{H}$ are again modeled by the double distribution ansatz (26). With regard to the symmetry properties of $\widetilde{H}$ the functions $\widetilde{h}_i$ now take the form

$$\begin{aligned}\tilde{h}_g(\beta) &= |\beta|\Delta g(|\beta|)\mathrm{sign}(\beta)\,,\\ \tilde{h}^q_{\rm sea}(\beta) &= \Delta q_{\rm sea}(|\beta|)\,,\\ \tilde{h}^q_{\rm val}(\beta) &= \Delta q_{\rm val}(\beta)\Theta(\beta)\,.\end{aligned} \tag{49}$$

For the powers n_i in the double distribution ansatz (26) the same values are taken as for the GPDs H^i; see (27). The decomposition of the double distribution into valence and sea contributions is made by [12]

$$\begin{aligned}\tilde{f}^q_{\rm val}(\beta,\alpha,t) &= \Big[\tilde{f}^q(\beta,\alpha,t) - \tilde{f}^q(-\beta,\alpha,t)\Big]\,\Theta(\beta)\,,\\ \tilde{f}^q_{\rm sea}(\beta,\alpha,t) &= \tilde{f}^q(\beta,\alpha,t)\Theta(\beta) + \tilde{f}^q(-\beta,\alpha,t)\Theta(-\beta)\,.\end{aligned} \tag{50}$$

The double distribution ansatz for $\widetilde{H}^g$ is incomplete, because in the moments of this GPD the highest power of ξ are lacking, which leads to difficulties with the analytic properties of the amplitudes [42]. We ignore this problem here, since the contributions from $\widetilde{H}^g$ seem to be unimportant.

Table 4. The parameters appearing in the expansion (30) of the polarized PDFs and the forward limits of E^a. The latter are taken from [9]. The expansion (30) provides a fit to the Blümlein–Böttcher PDFs [43] in the range $10^{-2} \leq \beta \leq 0.5$ and $4\,\mathrm{GeV}^2 \leq Q^2 \leq 40\,\mathrm{GeV}^2$. The powers $\tilde{\delta}$ are kept fixed in the fits to the PDFs

	$\Delta u_{\rm val}$	$\Delta d_{\rm val}$	$e^u_{\rm val}$	$e^d_{\rm val}$
$\tilde{\delta}$	0.48	0.48	0.48	0.48
$\tilde{c}_0$	$0.61 + 0.033\,L$	$-0.320 - 0.040\,L$	2.204	−3.114
$\tilde{c}_1$	$0.410 - 0.377\,L$	$-1.427 - 0.176\,L$	−2.204	8.096
$\tilde{c}_2$	$5.10 - 1.21\,L$	$0.692 - 0.068\,L$	0.0	−6.477
$\tilde{c}_3$	0.0	0.0	0.0	1.295

The required polarized parton distributions are taken from [43] and expanded according to

$$\tilde{h}_i(\beta) = \beta^{-\tilde{\delta}_i}\,(1-\beta)^{\,2n_i+1} \sum_{j=0}^{3} \tilde{c}_{ij}\beta^j\,, \tag{51}$$

using only integer powers. The resulting expansion parameters $\tilde{c}_i$ and $\tilde{\delta}_i$ are quoted in Table 4. It is expected that the a_1 Regge trajectory controls the low-x behavior of the polarized valence-quark PDFs. Since there are no recurrences of the $a_1(1260)$, we are forced to assume the standard value of $0.9\,\mathrm{GeV}^{-2}$ for the slope of the trajectory.[5] Combining this with the spin of the a_1, we obtain $\alpha_{a_1}(0) \simeq -0.36$ for the intercept. Such a low value is however in conflict with the small-x behavior[6] of the polarized valence-quark PDFs determined in [43], for which the power is rather about 0.7. As a compromise we therefore take the standard value of 0.48 for it. For the slope of the Regge trajectory we again take the value of 0.9 GeV2 and for its residue $\tilde{b}_{\rm val} = 0$.

The GPDs $\widetilde{H}^i$ are obtained from the functions f_i by the integral (29). They satisfy the relations

$$\begin{aligned} \widetilde{H}^g(-\bar{x},\xi,t) &= -\widetilde{H}^g(\bar{x},\xi,t)\,,\\ \widetilde{H}^q_{\rm sea}(-\bar{x},\xi,t) &= \widetilde{H}^q_{\rm sea}(\bar{x},\xi,t)\,, \end{aligned} \tag{52}$$

and

$$\widetilde{H}^q_{\rm val}(\bar{x},\xi,t) = 0\,, \quad -1 \leq \bar{x} < -\xi\,. \tag{53}$$

We checked that our proposed GPDs $\widetilde{H}_{\rm val}$ are in agreement with the data on the axial form factor for $-t \lesssim 0.6\,\mathrm{GeV}^2$ and with the low $-t$ (low x) behavior of $\widetilde{H}$ determined in [9]. In constrast to the situation for H, $\widetilde{H}^u_{\rm val}$ and $\widetilde{H}^d_{\rm val}$ have opposite signs as a consequence of the behavior of the polarized PDFs. The lowest moments of the latter are known from β decays (see, for instance, [43]). The usual assumption of a smooth behavior of the PDFs without a change of sign leads to opposite signs of $\Delta u_{\rm val}$ and $\Delta d_{\rm val}$.

As our numerical studies reveal, the gluon and sea-quark contributions to $\mathcal{M}^U$ are very small and compensate each other to a large extent, since the gluonic and sea-quark GPDs $\widetilde{H}$ have opposite signs. Their combined contributions are practically negligible. This is the reason why we quote only the expansion parameters of $\tilde{h}_i$ for the valence quarks in Table 4.

Neglecting as in the preceding sections proton helicity flips and photon–meson transitions other than $\mathrm{L} \to \mathrm{L}$ and $\mathrm{T} \to \mathrm{T}$, one can project out the unnatural parity amplitude for $\mathrm{T} \to \mathrm{T}$ transitions from a particular combination of SDMEs (see (43)):

$$U = \frac{1}{2}\left[1 - r^{04}_{00} - 2r^1_{1-1}\right] = \frac{2}{N_{\rm T} + \varepsilon N_{\rm L}} \mid M^U_{++,++} \mid^2\,. \tag{54}$$

This is the unnatural parity part of $N_{\rm T}$ scaled by $N_{\rm T} + \varepsilon N_{\rm L}$; see (42). Integrating over t one arrives at a cross section σ_U defined in analogy to $\sigma_{\rm T}$ in (7). Evaluating this cross section for ρ production from the amplitudes given in (3) and (48) and using the GPDs $\widetilde{H}$ described above, we find the results shown in Fig. 12. The cross section $\sigma_U(\rho)$ is rather small but in agreement with the preliminary HERMES result [35, 36] at $Q^2 = 2.88\,\mathrm{GeV}^2$ within an admittedly large error. For larger energies our approach will lead to even smaller values for σ_U, since the valence-quark contribution disappears and, as we mentioned above, the combined gluon and sea contribution is very small (the typical size of gluon plus sea-quark contribution to $\sigma_U(\rho)$ is 0.013 nb). We note that for ρ production, the H1 data [25] provide values for σ_U that are compatible with zero (e.g. at $Q^2 = 3\,\mathrm{GeV}^2$, $\sigma_U/\sigma = 0.03 \pm 0.07$), while the ZEUS results [24] are about 1.5σ above zero (e.g. at $Q^2 \simeq 3.4\,\mathrm{GeV}^2$, $\sigma_U/\sigma = 0.03 \pm 0.02$). Both experimental results are in agreement with our estimates within errors. An immediate consequence of the cancellation of gluon and sea contributions to the unnatural parity amplitude is that σ_U for ϕ production is very small – in fact compatible with zero. This is in agreement with the preliminary HERMES data [37] and with the H1 data [32]. Thus, there is indication from both theory and experiment that σ_U for ρ and ϕ production is small. Its neglect in $\sigma_{\rm T}$ seems to be justified. A larger cross section σ_U is to be expected for ω production, because the combination $e_u\widetilde{H}^u_{\rm val} + e_d\widetilde{H}^d_{\rm val}$ occurs (see (4)), which is larger than $e_u\widetilde{H}^u_{\rm val} - e_d\widetilde{H}^d_{\rm val}$ given the relative sign of $\widetilde{H}^u_{\rm val}$ and $\widetilde{H}^d_{\rm val}$.

[5] Accepting exchange degeneracy for the a_1 and $\eta_2(1617)$ trajectories the slope of the trajectory is fixed by the meson spectrum and is indeed $0.9\,\mathrm{GeV}^{-2}$.

[6] Whether this is a consequence of lack of low-x data in the PDF analysis or due to disregarded high-lying Regge cuts, is unknown at present.

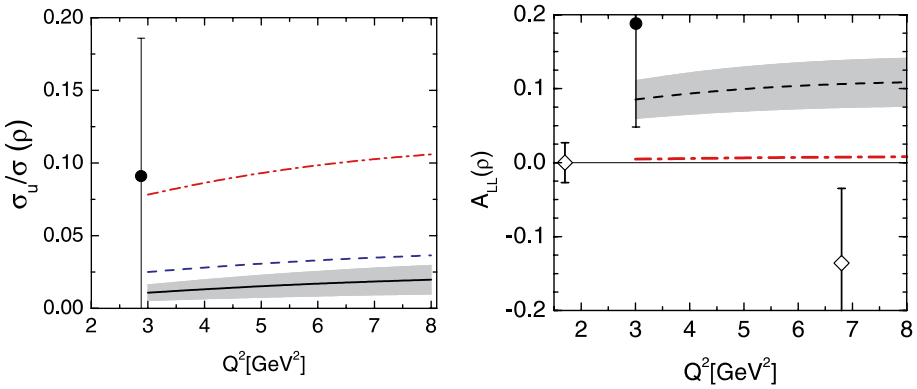

Fig. 12. *Left*: the ratio of σ_U and σ for ϱ production versus Q^2 at $W = 5\,\text{GeV}$. The data are taken from HERMES [35, 36]. The *solid* (*dashed*, *dash-dotted*) *line* represents our estimate (obtained with $e_u H^u_{\rm val} + e_d H^d_{\rm val}$, with $e_u H^u_{\rm val} - e_d H^d_{\rm val}$); see text. *Right*: the helicity correlation $A_{\rm LL}$ for ϱ production at $W = 5(\,10)\,\text{GeV}$ *dashed* (*dash-dotted*) *line*. The data are taken from COMPASS [48] and HERMES [49]. For other notation refer to Figs. 3 and 4

One may wonder whether or not it is possible to generate a value for σ_U as large as, say, the face value of the preliminary HERMES result [35, 36] by using GPDs constructed from the polarized PDFs via the double distribution ansatz. In order to examine this issue we recall that the polarized PDFs are the difference of PDFs for helicity parallel and anti-parallel to that one of the proton, while the unpolarized PDFs represent their sum. Suppose the gluon and sea-quark contributions still cancel and assume now that the helicity-parallel distributions dominate, which, in the limit $x \to 1$, follows from QCD [44]. In this case the double distribution ansatz leads to $\widetilde{H}^a_{\rm val} = H^a_{\rm val}$. Admittedly this is an extreme example, since in all analyses [43, 45, 46] the polarized d-quark distribution is negative. Another, more moderate example is set by the assumption $\widetilde{H}^u_{\rm val} = H^u_{\rm val}$ and $\widetilde{H}^d_{\rm val} = -H^d_{\rm val}$, implying d quarks with dominantly anti-parallel helicity. The results obtained from these two scenarios are also shown in Fig. 12. Obviously, it seems difficult to obtain agreement with the HERMES result [35, 36] with GPDs constructed from the double distribution ansatz, except when extreme scenarios are realized in nature.

The size of the amplitude $\mathcal{M}^U$ can be elucidated further by considering the initial state helicity correlation $A_{\rm LL}$, which can be measured with a longitudinally polarized beam and target. In contrast to cross sections and SDMEs, where the corrections are bilinear in the $\mathcal{M}^U$ terms and, hence, very small, the leading term in $A_{\rm LL}$ is an interference between the $\mathcal{M}^N$ and the $\mathcal{M}^U$ amplitudes. In fact, with the help of parity conservation as well as (9) and (10), one obtains [1]

$$A_{\rm LL}[ep \to eVp] = 4\sqrt{1-\varepsilon^2}\,\frac{\text{Re}\left[\mathcal{M}^N_{++,++}\mathcal{M}^{U*}_{++,++}\right]}{N_{\rm T} + \varepsilon N_{\rm L}}\,. \tag{55}$$

We stress that here the target polarization is specified relative to the virtual photon direction, while in experiment it is usually defined with respect to the lepton beam direction. The conversion from our specification to the one used in experiments leads to a factor $\cos\theta_\gamma$ in (55) [47], where θ_γ denotes the angle describing the rotation in the lepton plane from the direction of the incoming lepton to the one of the virtual photon. This angle is given by [47]

$$\cos\theta_\gamma = \sqrt{1-\gamma^2\frac{1-y-y^2\gamma^2/4}{1+\gamma^2}} \simeq 1 - \frac{1}{2}\gamma^2(1-y)\,. \tag{56}$$

The two parameters appearing in (56) are $y = (W^2 + Q^2 - m^2)/(s - m^2)$, one of the conventional variables of electroproduction, and $\gamma = 2x_{\rm Bj}m/Q$. In the kinematical situation of interest γ is very small and, hence, $\cos\theta_\gamma \simeq 1$. According to (18) $A_{\rm LL}$ is of order $\langle k_\perp^2\rangle/Q^2$, and, therefore, expected to be very small. In Fig. 12 our results for ρ production are shown at $W = 5$ and $10\,\text{GeV}$. For the lower energy the valence-quark contribution generates values for $A_{\rm LL}$ of about 0.1, while at 10 GeV only extremely small values are found. The valence-quark contribution has nearly disappeared at that energy and, as we mentioned above, the gluon and sea-quark contributions cancel each other to a large extent. For instance, at $W = 5\,\text{GeV}$ and $Q^2 = 3\,\text{GeV}^2$, $A_{\rm LL}(\rho)$ changes by -0.002 if the gluon and sea quarks are neglected. Because of the very small combined gluon and sea contributions we also predict very small values of $A_{\rm LL}(\phi)$. For instance, at $W = 5(\,10)\,\text{GeV}$ and $Q^2 = 3\,\text{GeV}^2$, $A_{\rm LL}(\phi) = -0.002(-0.007)$.

Recently, the COMPASS collaboration has measured $A_{\rm LL}$ for ρ production [48]. For Q^2 less than $2\,\text{GeV}^2$ COMPASS observes very small values for $A_{\rm LL}$, which are compatible with zero. Their only data point for which its Q^2 is sufficiently large for application of the handbag approach is inconclusive, because of its extremely large error; it is at variance with our results by about 1σ; see Fig. 12. The HERMES results on this observable for ρ and ϕ production [49] is in agreement with our predictions. The SMC experiment [50] observes a double spin asymmetry for ρ production at $W = 15\,\text{GeV}$ that is compatible with our results within large errors. In passing, we remark that $A_{\rm LL}$ is sensitive to the relative phase δ_{NU} between the amplitudes $\mathcal{M}^N_{++,++}$ and $\mathcal{M}^U_{++,++}$. Therefore, a large value of

σ_U is not necessarily in contradiction with a small value of $A_{\rm LL}$, provided the phase is near 90°. Nevertheless, in our approach the phase is small. For instance, at $W = 5\,\text{GeV}$ and $Q^2 = 3\,\text{GeV}^2$ we find $\delta_{NU} = 3.7°$, i.e. a large value of σ_U would go along with a large value of $A_{\rm LL}$ in our approach. For instance, a scenario with $\widetilde{H}^a_{\rm val} = H^a_{\rm val}$ leads to $A_{\rm LL}(\rho) = 0.14$ for this kinematical point of reference.

Let us return to the issue of the size of the combined gluon and sea contribution to the unnatural parity amplitude. Up to know we have assumed that this combined contribution is very small as follows from the double distribution ansatz using current polarized PDFs. One may wonder whether these PDFs are really correct or whether the smallness of the combined gluon and sea contribution is perhaps a special feature of our double distribution ansatz for $\widetilde{H}$. First we note that in all current analyses of the polarized PDFs [43, 45, 46] Δg and the polarized sea have opposite signs and are rather small in magnitude.[7] In particular a large positive Δg is in conflict with measurements of the $A_{\rm LL}$ asymmetry in the production of jets [51] and π^0 mesons [52] in inclusive proton–proton collisions. A negative polarized sea is for instance seen in the HERMES semi-inclusive deep inelastic scattering data [53]. Thus, we think that the main features of the polarized PDFs are correct. A small combined gluon and sea contribution from $\widetilde{H}$ seems to be required by the relevant data too. Leaving aside the HERMES results on σ_U and $A_{\rm LL}$ for ρ production, which receive contributions from $\widetilde{H}_{\rm val}$, we note that all other pertinent data are small and in most cases compatible with zero. These data are $\sigma_U(\rho)$ from H1 [25] and ZEUS [24], the same cross section for ϕ production from HERMES [37] and H1 [32] and finally the $A_{\rm LL}$ data from Compass [48] and SMC [50]. Thus, scenarios in which the combined gluon and sea-quark contribution is large in magnitude seem to be excluded by the current data. Our double distribution ansatz for $\widetilde{H}^g$ and $\widetilde{H}_{\rm sea}$, as naive it may be, qualitatively reproduces the main features of the data.

7 Proton helicity flip

The analysis of observables for vector-meson electroproduction measured with a transversely polarized proton target requires the proton helicity-flip amplitude. The handbag contribution to this amplitude is given by

$$\mathcal{M}^{Ni}_{\mu-,\mu+}(V) = -\frac{e}{2}\,\frac{\sqrt{-t}}{2m}\sum_a e_a \mathcal{C}^{\rm a}_V \times \int_{\bar{x}_i}^1 {\rm d}\bar{x}\,\left[\mathcal{H}^{Vi}_{\mu+,\mu+} + \mathcal{H}^{Vi}_{\mu-,\mu-}\right] E^i(\bar{x},\xi,t)\,, \tag{57}$$

where $t_{\rm min}$ is ignored. Our choice of the phase of this amplitude is in accord with the conventions exploited in [41, 47]. In general there is also a contribution from the GPD $\widetilde{E}$, feeding the amplitude $\mathcal{M}^{Ui}_{+-,++}$. It is expected to be small and neglected in our estimate of the size of the proton helicity-flip amplitude. The evaluation of $\mathcal{M}^N$ for proton helicity flip is analogous to that of the non-flip amplitude (3), except that the convolution is now to be performed with the GPD E instead of H. The construction of E through double distributions is also analogous to that of H; see Sect. 3. The only but crucial difference is that the forward limit $e(x) = E(x,0,0)$ is inaccessible in deep inelastic lepton–nucleon scattering. However, the forward limits of the valence-quark GPDs have been determined phenomenologically in the form factor analysis performed in [9]. The parameters of $e^u_{\rm val}$ and $e^d_{\rm val}$ expanded according to (51), are taken from [9]. They are quoted in Table 4 at a scale of $4\,\text{GeV}^2$. For other scales these functions are unknown, which does not matter here since we will estimate proton helicity flip only for photon virtualities near that value. Note that in contrast to $u_{\rm val}$ and $d_{\rm val}$, $e^u_{\rm val}$ and $e^d_{\rm val}$ have opposite signs. This is due to the fact that they are normalized by

$$\int_0^1 {\rm d}x\; {\rm e}^a_{\rm val}(x) = \kappa_a\,, \tag{58}$$

where κ^a gives the contribution of quark flavor a to the anomalous magnetic moment of the proton ($\kappa_u \simeq 1.67$, $\kappa_d \simeq -2.03$). The forward limits of E for gluons and sea quarks are unknown. But there is a sum rule,

$$\int_0^1 {\rm d}x\, x e^g(x) = -\sum_a \int_0^1 {\rm d}x x e^a_{\rm val}(x) - 2\sum_a \int_0^1 {\rm d}x\, x e^{\bar{a}}(x)\,, \tag{59}$$

which follows from a combination of Ji's sum rule and the momentum sum rule of deep inelastic lepton–nucleon scattering [12]. Neglecting a possible difference between e^s and $e^{\bar{s}}$, we can evaluate the valence-quark term in the sum rule (59) from the GPDs specified in Table 4. We obtain

$$\sum_a \int_0^1 {\rm d}x\, x e^a_{\rm val}(x) = 0.008 \pm 0.007\,. \tag{60}$$

This signals a remarkable compensation between the second moments of $e^u_{\rm val}$ and $e^d_{\rm val}$

$$\frac{\int_0^1 {\rm d}x\, x[e^u_{\rm val} + e^d_{\rm val}]}{\int_0^1 {\rm d}x\, x[e^u_{\rm val} - e^d_{\rm val}]} \simeq 0.026\,, \tag{61}$$

which is even stronger than that of their first moments ($(\kappa_u + \kappa_d)/(\kappa_u - \kappa_d) \simeq 0.1$). The error in (60) has been estimated from those quoted in [9]. Hence, the moment of e^g in (60) is only about as large as the sum of the sea-quark moments. This is to be contrasted with the situation for H, where the corresponding gluon moment is more than four times larger than the sum of the sea-quark ones. Another argument that points into the same direction is the behavior of the gluon (or pomeron) Regge trajectory. As is well known, this trajectory couples mainly to the proton helicity-non-flip vertex, while the flip coupling is very

[7] A negative Δg is also discussed in [45].

small. It is hard to find phenomenological evidence for a non-zero flip coupling [54]. Thus, the relative importance of gluon and valence-quark GPDs is very different for E and H. It seems unlikely that E^g plays an analogously prominent role as H^g. In a first step we therefore assume that, for HERMES kinematics, proton helicity flip is dominated by the valence quarks [16]. Since the same Regge poles contribute to E and H, we therefore use the standard valence-quark trajectory here as well and assume $b^e_{\rm val} = 0$, too. With regard to this situation we cannot estimate the size of proton helicity flip for ϕ production, but we expect it to be very small. We stress that due to the opposite signs of $E^u_{\rm val}$ and $E^d_{\rm val}$, their contribution to ρ production off protons, $\propto e_u E^u_{\rm val} - e_d E^d_{\rm val}$, is much smaller than that from the corresponding contribution of $H^a_{\rm val}$. This provides an additional justification for the neglect of E in the proton helicity-non-flip amplitude (see discussion after (2)). An interesting case is ω production, since for this case the combinations $e_u E^u_{\rm val} + e_d E^d_{\rm val}$ and $e_u H^u_{\rm val} + e_d H^d_{\rm val}$ occur. The first combination is larger, the second one smaller than for ρ production and, hence, a markedly larger ratio of proton helicity flip and non-flip is expected for ω production. For instance, at $Q^2 = 4\,\text{GeV}^2$ and $W = 5\,\text{GeV}$ the flip/non-flip ratio of the absolute values of the ω amplitudes is about 13 times larger than the corresponding ratio for ρ production.

Recently the formalism for the SDMEs in the case of a proton target polarized perpendicular ('normal') with respect to the plane in which the scattering $\gamma^* p \to V p$ takes place has been developed [41]. These SDMEs are denoted by $n^{\sigma\sigma'}_{\mu\mu'}$ and are related to bilinear combinations of the amplitudes for the helicities μ, μ' and σ, σ' of the virtual photon and the meson, respectively:

$$n^{\sigma\sigma'}_{\mu\mu'} = \frac{1}{N_{\rm T} + \varepsilon N_{\rm L}} \sum_{\nu'} \Big[\mathcal{M}_{\sigma\nu',\mu+}\, \mathcal{M}^*_{\sigma'\nu',\mu'-} - \mathcal{M}_{\sigma\nu',\mu-}\, \mathcal{M}^*_{\sigma'\nu',\mu'+} \Big] \,. \quad (62)$$

If one neglects the amplitudes $\mathcal{M}^U$ in accord with our findings described in Sect. 6, as well as the helicity-flip transitions $\gamma^* \to V$ only the SDMEs

$$n^{\mu\mu'}_{\mu\mu'} = \frac{2}{N_{\rm T} + \varepsilon N_{\rm L}} \sum_{\nu'} \mathcal{M}^N_{\mu\nu',\mu+} \mathcal{M}^{N*}_{\mu'\nu',\mu'-} \,, \quad (63)$$

are non-zero. Explicitly these SDME read

$$\begin{aligned} n^{00}_{00} &= \frac{4\mathrm{i}}{N_{\rm T} + \varepsilon N_{\rm L}} \mathrm{Im}\left[\mathcal{M}^N_{0-,0+} \mathcal{M}^{N*}_{0+,0+}\right] \,, \\ n^{++}_{++} &= n^{-+}_{-+} = \frac{4\mathrm{i}}{N_{\rm T} + \varepsilon N_{\rm L}} \mathrm{Im}\left[\mathcal{M}^N_{+-,++} \mathcal{M}^{N*}_{++,++}\right] \,, \\ n^{0+}_{0+} &= -(n^{+0}_{+0})^* \\ &= \frac{2}{N_{\rm T} + \varepsilon N_{\rm L}} \left[\mathcal{M}^N_{0-,0+}\, \mathcal{M}^{N*}_{++,++} - \mathcal{M}^N_{0+,0+}\, \mathcal{M}^{N*}_{+-,++}\right] . \end{aligned} \quad (64)$$

For non-zero SDMEs $n^{\mu\mu'}_{\mu\mu'}$ phase differences between the proton helicity-flip and -non-flip amplitudes are mandatory. Such phase differences are provided by the handbag approach, since the non-flip amplitudes are built up by gluons and quarks, while the flip amplitudes receive only contributions from the valence quarks in our model for the GPD E. Indeed we obtain the values 38.8° and 34.7° for the phase between the proton flip and non-flip amplitudes in the case of longitudinal and transverse photon polarization, respectively. In Fig. 13 the SDMEs (64) are shown versus Q^2 at $W = 5\,\text{GeV}$, and the trivial factor $\sqrt{-t}/2m$, see (57), is pulled out and t set to zero otherwise. The scaled SDMEs are small, of the order of five percent. These SDMEs will be measured by HERMES.

One may also consider transverse proton polarization lying in the $\gamma^* p \to V p$ plane ('sideways'). In this case SDMEs, denoted by $s^{\sigma\sigma'}_{\mu\mu'}$ [41], occur that are analogous to (62) but with a plus sign between the two terms. The SDMEs $s^{\mu\mu'}_{\mu\mu'}$ for photon–meson helicity non-flip are given by products of two small amplitudes, $\mathcal{M}^N$ for proton helicity flip and $\mathcal{M}^U$. They are therefore very small in our approach.

Finally, we estimate the asymmetry A_{UT} of $ep \to eVp$ for a transversely polarized target, normal to the $\gamma^* p \to V p$ scattering plane. It is measured as the $\sin(\phi - \phi_S)$ moment

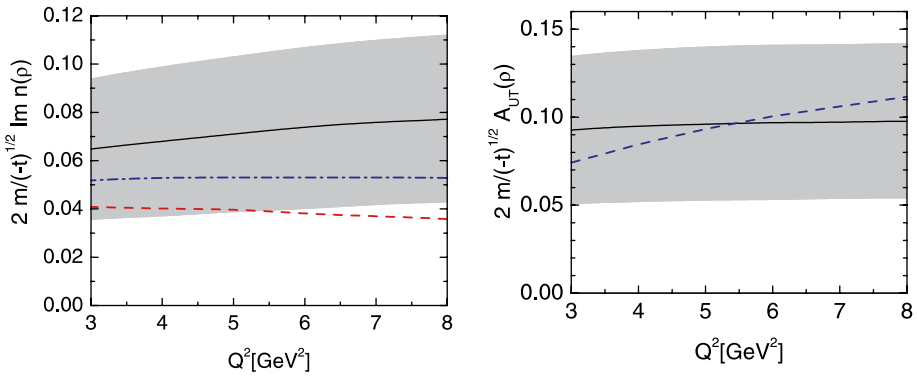

Fig. 13. *Left*: the imaginary parts of the SDMEs n^{00}_{00} (*solid*), n^{++}_{++} (*dashed*) and n^{0+}_{0+} (*dash-dotted line*), scaled by $2m/\sqrt{-t}$, for ϱ production versus Q^2 at $W = 5\,\text{GeV}$. The error band is only shown for n^{00}_{00}. *Right*: the asymmetry A_{UT}, scaled by $2m/\sqrt{-t}$, for ϱ production versus Q^2 at $W = 5\,\text{GeV}$. The *dashed line* represents the leading-twist contribution

of the electroproduction cross section where ϕ is the azimuthal angle between the lepton and hadron plane and ϕ_S the azimuthal angle of the target spin vector defined with respect to the direction of the virtual photon [41]. As for the asymmetry $A_{\rm LL}$ the conversion of this spin vector into the one used in the experimental setup where the target polarization is specified relative to the lepton beam, again leads to a factor $\cos\theta_\gamma$ in principle. According to the discussion following (56) it is replaced by one. In the handbag approach the dominant contribution to this asymmetry reads

$$A_{UT}(ep\to eVp) = 4\frac{\mathrm{Im}\left[\mathcal{M}^{N}_{+-,++}\mathcal{M}^{N*}_{++,++}\right]+\varepsilon\mathrm{Im}\left[\mathcal{M}^{N}_{0-,0+}\mathcal{M}^{N*}_{0+,0+}\right]}{N_{\rm T}+\varepsilon N_{\rm L}}\,. \tag{65}$$

It is just the imaginary part of the sum of n^{++}_{++} and εn^{00}_{00} and is also proportional to $\sqrt{-t}/2m$. We again pull out the latter factor and display the scaled asymmetry, evaluated at $t=0$, in Fig. 13. We obtain a positive asymmetry. In contrast to $A_{\rm LL}$ it is finite to leading-twist order, which is obtained from (65) by neglecting the contributions from transverse photons and evaluating those from longitudinal photons in collinear approximation. For comparison, the leading-twist contribution is also shown in Fig. 13. It is not too different from the full result. A preliminary HERMES result [55] for ρ production, integrated on the range $0\geq -t\geq 0.4\,\mathrm{GeV}^2$, is -0.033 ± 0.058 at $Q^2=3.07\,\mathrm{GeV}^2$ and $W=5\,\mathrm{GeV}$, while we find 0.02 ± 0.01 for this kinematical situation. Note that the scaled asymmetry is still t dependent, although mildly so. Ignoring this and integrating just $\sqrt{-t}$ one makes an error of about 10% at $Q^2\simeq 3$–$4\,\mathrm{GeV}^2$. For ω production A_{UT} is about 10 times larger than for ρ production. For ϕ production, on the other hand, we expect a very small asymmetry since the gluon and sea contributions are not only small but cancel each other to some extent, see (59).

The asymmetry A_{UL} for an unpolarized beam and a longitudinally polarized target is given by the same expression as A_{UT}. Only the mentioned conversion factor $\cos\theta_\gamma$ is to be replaced by $\sin\theta_\gamma$ which is very small [47]. The beam asymmetry A_{LU} obtained with a logitudinally polarized beam and an unpolarized target is zero given that helicity-flip $\gamma^*\to V$ transitions can be neglected.

8 Summary

Together with [3] this work gives an exhaustive description of light vector-meson electroproduction within the handbag approach for a wide range of kinematics reaching from the HERMES up to the HERA kinematical settings. Our handbag approach includes power corrections which suppress the leading-twist amplitude for $\gamma^*_{\rm L}\to V_{\rm L}$ transitions and allows for a calculation of the transverse amplitude $\gamma^*_{\rm T}\to V_{\rm T}$. In order to specify our handbag approach fully we have to mention the soft physics input, namely the GPDs that are constructed from PDFs with the help of double distributions, and the light-cone wave functions for the mesons. GPDs and wave functions affect the handbag amplitudes differently and can therefore be disentangled. The wave functions provide effects of order $\langle\mathbf{k}^2_\perp\rangle/Q^2$ controlled by the transverse size parameter a_V while the GPDs mainly influence the $x_{\rm Bj}$ dependence of the amplitudes or, at fixed Q^2, the W dependence. Besides the dominant contributions from the GPD H ('natural parity' contribution) we also estimated effects from the GPDs $\widetilde{H}$ ('unnatural parity' contribution) and E controlling the proton helicity-flip amplitudes. These effects are generally small. With our analysis we achieve a very good description of the HERA, HERMES and COMPASS data on the separated and non-separated cross sections for ρ and ϕ electroproduction, on the ratio $\sigma_{\rm L}/\sigma_{\rm T}$, on the SDMEs and on some spin asymmetries. The only problem we observed is that the relative phase between the longitudinal and transverse amplitudes seems to be larger in experiment, in particular in the HERMES experiment [35, 36], than our handbag approach predicts. The neglect of contributions from transitions other than $\gamma^*_{\rm L}\to V_{\rm L}$ and $\gamma^*_{\rm T}\to V_{\rm T}$ to the cross sections seems to be justified. Only little contributions from $\gamma^*_{\rm T}\to V_{\rm L}$ transitions are to be observed in some of the SDMEs experimentally. We note that in [56] the longitudinal amplitude has also been analyzed within the handbag approach. The main difference to our work is that in [56] the gluonic contribution is treated in leading-log approximation [57] and added incoherently to the quark amplitudes. This line of action underestimates the gluonic contribution at low energies.

The applicability of our approach is limited to $Q^2\gtrsim 3$–$4\,\mathrm{GeV}^2$, $W\gtrsim 4$–$5\,\mathrm{GeV}$ and $x_{\rm Bj}\lesssim 0.2$. The restriction of Q^2 is due to the mentioned – and still unsettled – difficulties with higher order perturbative corrections as well as due to the neglected corrections of order m^2/Q^2 and $-t/Q^2$. There may be also power corrections of other dynamical origin which become large at low Q^2. The restriction of W has its origin in the asymmetric minimum the cross sections exhibit at $W\simeq 3$–$4\,\mathrm{GeV}$. While the cross sections [24, 25, 34, 58] mildly increase towards larger W, they [35, 36, 59, 60] increase sharply in the opposite direction. In fact they rise by nearly an order of magnitude between $W\simeq 4$ and $2\,\mathrm{GeV}$. Obviously, a new dynamical mechanism seems to set in and the handbag physics is perhaps not applicable here. On the other side, it dominates for $W\gtrsim 4\,\mathrm{GeV}$. The mild increase of the cross sections with energy beyond the minimum is well described by the handbag physics as the results presented in this article and in [3] reveal. The restriction of $x_{\rm Bj}$ is of difference quality. It allows to neglect contributions of order $x^2_{\rm Bj}$ or ξ^2, e.g. in (1), which simplifies the analysis of vector-meson electroproduction strongly.

Acknowledgements. We thank A. Borissov, M. Diehl, N. d'Hose, A. Levy, W.-D. Nowak and A. Sandacz for discussions. We are also grateful to the HERMES and COMPASS collaborations for permission to use preliminary data. This work has been supported in part by the Russian Foundation for Basic Research, Grant 06-02-16215, the Integrated Infrastructure Ini-

tiative "Hadron Physics" of the European Union, contract No. 506078 and by the Heisenberg–Landau program.

References

1. S.V. Goloskokov, P. Kroll, Eur. Phys. J. C **42**, 281 (2005) [hep-ph/0501242]
2. J. Botts, G. Sterman, Nucl. Phys. B **325**, 62 (1989)
3. S.V. Goloskokov, P. Kroll, Eur. Phys. J. C **50**, 829 (2007) [hep-ph/0611290]
4. L. Mankiewicz, G. Piller, Phys. Rev. D **61**, 074013 (2000) [hep-ph/9905287]
5. I.V. Anikin, O.V. Teryaev, Phys. Lett. B **554**, 51 (2003) [hep-ph/0211028]
6. J. Pumplin, D.R. Stump, J. Huston, H.L. Lai, P. Nadolsky, W.K. Tung, JHEP **0207**, 12 (2002) [hep-ph/0201195]
7. D. Mueller et al., Fortschr. Phys. **42**, 101 (1994) [hep-ph/9812448]
8. A.V. Radyushkin, Phys. Lett. B **449**, 81 (1999) [hep-ph/9810466]
9. M. Diehl, T. Feldmann, R. Jakob, P. Kroll, Eur. Phys. J. C **39**, 1 (2005) [hep-ph/0408173]
10. A.V. Radyushkin, Phys. Lett. B **385**, 333 (1996) [hep-ph/9605431]
11. J.C. Collins, L. Frankfurt, M. Strikman, Phys. Rev. D **56**, 2982 (1997) [hep-ph/9611433]
12. M. Diehl, Phys. Rep. **388**, 41 (2003) [hep-ph/0307382]
13. M. Diehl, W. Kugler, A. Schafer, C. Weiss, Phys. Rev. D **72**, 034034 (2005) [hep-ph/0506171]
14. M. Diehl, W. Kugler, A. Schafer, C. Weiss, Phys. Rev. D **72**, 059902 (2005) [Erratum]
15. D.Y. Ivanov, L. Szymanowski, G. Krasnikov, JETP Lett. **80**, 226 (2004) [Pisma Zh. Eksp. Teor. Fiz. **80**, 255 (2004)] [hep-ph/0407207]
16. M. Diehl, W. Kugler, arXiv:0708.1121 [hep-ph]
17. D.Y. Ivanov, to be published in the Proc. EDS07 conference, Hamburg (2007)
18. S. Catani, F. Hautmann, Nucl. Phys. B **427**, 475 (1994) [hep-ph/9405388]
19. R. Jakob, P. Kroll, Phys. Lett. B **315**, 463 (1993) [hep-ph/9306259]
20. R. Jakob, P. Kroll, Phys. Lett. B **319**, 545 (1993) [Erratum]
21. P.V. Landshoff, J.C. Polkinghorne, R.D. Short, Nucl. Phys. B **28**, 225 (1971)
22. R.P. Feynman, Photon-Hadron Interactions (W.A. Benjamin, INC., Reading, Massachusetts, 1972)
23. M.V. Polyakov, C. Weiss, Phys. Rev. D **60**, 114017 (1999) [hep-ph/9902451]
24. ZEUS Collaboration, S. Chekanov et al., arXiv:0708.1478 [hep-ex]
25. H1 Collaboration, C. Adloff et al., Eur. Phys. J. C **13**, 371 (2000) [hep-ex/9902019]
26. ZEUS Collaboration, S. Chekanov et al., Nucl. Phys. B **718**, 3 (2005) [hep-ex/0504010]
27. A.V. Vinnikov, hep-ph/0604248
28. P. Ball, V.M. Braun, Phys. Rev. D **54**, 2182 (1996) [hep-ph/9602323]
29. M.A. Shifman, M.I. Vysotsky, Nucl. Phys. B **186**, 475 (1981)
30. M. Glück, C. Pisano, E. Reya, Eur. Phys. J. C **50**, 29 (2007) [hep-ph/0610060]
31. M. Glück, E. Reya, A. Vogt, Eur. Phys. J. C **5**, 461 (1998) [hep-ph/9806404]
32. H1 Collaboration, C. Adloff et al., Phys. Lett. B **483**, 360 (2000) [hep-ex/0005010]
33. H1 Collaboration, S. Aid et al., Nucl. Phys. B **468**, 3 (1996) [hep-ex/9602007]
34. ZEUS Collaboration, J. Breitweg et al., Eur. Phys. J. C **6**, 603 (1999) [hep-ex/9808020]
35. HERMES Collaboration, A. Borissov, Proc. "Diffraction 06", PoS (DIFF2006) 014
36. HERMES Collaboration, B. Marianski, Proc. "DIS 2006", (World Scientific, Singapore, 2007)
37. HERMES Collaboration, A. Borissov, Proc. of DSPIN-07, to be published
38. COMPASS Collaboration, D. Neyret, preliminary data presented at SPIN2004, Trieste, Italy
39. ZEUS Collaboration, J. Breitweg et al., Eur. Phys. J. C **12**, 393 (2000) [hep-ex/9908026]
40. K. Schilling, G. Wolf, Nucl. Phys. B **61**, 381 (1973)
41. M. Diehl, JHEP **0709**, 064 (2007) [hep-ph/07041565]
42. M. Diehl, D.Y. Ivanov, arXiv:0707.0351 [hep-ph]
43. J. Blümlein, H. Böttcher, Nucl. Phys. B **636**, 225 (2002) [hep-ph/0203155]
44. S.J. Brodsky, M. Burkardt, I. Schmidt, Nucl. Phys. B **441**, 197 (1995) [hep-ph/9401328]
45. E. Leader, A.V. Sidorov, D.B. Stamenov, Phys. Rev. D **75**, 074027 (2007) [hep-ph/0612360]
46. M. Hirai, S. Kumano, N. Saito, Phys. Rev. D **74**, 014015 (2006) [hep-ph/0603213]
47. M. Diehl, S. Sapeta, Eur. Phys. J. C **41**, 515 (2005) [hep-ph/0503023]
48. COMPASS Collaboration, V.Y. Alexakhin et al., Eur. Phys. J. C **52**, 255 (2007) [hep-ex/0704.1863]
49. HERMES Collaboration, A. Airapetian et al., Eur. Phys. J. C **29**, 171 (2003) [hep-ex/0302012]
50. Spin muon Collaboration, A. Tripet, Nucl. Phys. Proc. Suppl. **79**, 529 (1999) [hep-ex/9906008]
51. STAR Collaboration, K. Kowalik, hep-ex/0706.2667
52. PHENIX Collaboration, A. Adare et al., Phys. Rep. D **76**, 051106 (2007) arXiv:0704.3599 [hep-ex]
53. HERMES Collaboration, A. Airapetian et al., Phys. Rev. D **71**, 012003 (2005) [hep-ex/0407032]
54. A. Donnachie, Phys. Lett. B **611**, 255 (2005) [hep-ph/0412085]
55. HERMES Collaboration, A. Rostomyan, Proc. "DIS 2007", (World Scientific, Singapore, 2007)
56. M. Vanderhaeghen, P.A.M. Guichon, M. Guidal, Phys. Rev. D **60**, 094017 (1999) [hep-ph/9905372]
57. L. Frankfurt, W. Koepf, M. Strikman, Phys. Rev. D **54**, 3194 (1996) [arXiv:hep-ph/9509311]
58. E665 Collaboration, M.R. Adams et al., Z. Phys. C **74**, 237 (1997)
59. D.G. Cassel et al., Phys. Rev. D **24**, 2787 (1981)
60. CLAS Collaboration, C. Hadjidakis et al., Phys. Lett. B **605**, 256 (2005) [hep-ex/0408005]